The GREAC cell used to establish constitutive models for powder type materials

John F. Moxnes and Øyvind Frøyland

Forsvarets forskningsinstitutt/Norwegian Defence Research Establishment (FFI)

21 Januay 2009

FFI-rapport 2009/00162

1072

P: ISBN 978-82-464-1523-9
E: ISBN 978-82-464-1524-6

Keywords

Glasspulver/Glass powder

Materialmodell/Material model

Ammunisjon/Ammunition

Strekklapp/Strain gauges

Approved by

Hege Kristin Jødahl	Project manager
Jan Ivar Botnan	Director

English summary

In this report a theoretical and experimental study of a glass powder (diameter of 40-80 μm) is made to establish a constitutive material model by using the GREAC (Gauged REActive Confinement) cell. The GREAC cell is simply a hollow cylinder were the test material is inserted and compressed axially. We show how an algorithm can be used to establish constitutive material models from the output data from the experiment. The algorithm use measurements of the axial force, the axial displacement of the glass powder and the axial and hoop strain measured at the outer surface of the GREAC cell. By comparing the assumptions in the model with well known materials we test the quality of the model. A check of the quality/accuracy of the measurements have also been done. A finite element analysis has been performed by using SolidWorks with COSMOSWorks.

Sammendrag

Vi gjennomfører en teoretisk og eksperimentell studie for å etablere en konstitutiv modell for glasspulver (diameter på ca. 40-80 μm). Den såkalte GREAC (Gauged REActive Confinement) cellen brukes i den teoretiske analysen. GREAC cellen er i prinsippet en hul stålsylinder hvor testmaterialet settes og sammenpresses aksialt med et stempel. Vi viser hvordan man ved hjelp av en algoritme kan etablere en materialmodell fra måledata. Algoritmen bruker de målte kreftene i topp og bunn av testmaterialet, aksiell sammenpressing av testmaterialet og den tangentielle og langsgående tøyningen på utsiden av stålsylinderen. Ved å sammenligne våre antagelser i materialmodellen med målinger på velkjente materialer har vi fått en kvalitetssjekk av materialmodellen (kapittel 5). I tillegg har vi sjekket kvaliteten/nøyaktigheten på målingene (kapittel 6 og 7). En analyse av GREAC oppsettet med endelige elementers metode ble gjort i SolidWorks (CAD) med analyseverktøyet COSMOSWorks.

Contents

1 Introduction

Good material models are requisite for applying computer simulations. To achieve predictability of these mathematical material models, they are usually tuned to experimental data from tests very different from the actual setup for a specific computer simulation. The reason for this procedure is that most material models have many free parameters, which always can be tuned to match a specific problem. By establishing material data from one type of test, and achieving good simulation results for very different types of tests, good credibility of a material model is achieved.

Typical static scientific tests for establishing constitutive models are the simple compression test, the bending test and the unilateral compression test. Extensive engineering use is also made of the hardness test. The unilateral compression test of powder type materials is usually performed by using a variant of the so called GREAC (Gauged REActive Confinement) cell, where the test material is confined inside a hollow steel cylinder. During compression a force applies through a piston that compresses and compacts the material axially in the cylinder. The axial force acting on the sample material is measured on the top piston (applied force) and bottom piston (transmitted force). In general the transmitted force is different from the applied force due to friction between the sample and the cylinder. The radial stress in the material is not directly measured but calculated from measurements of the strains from two strain gauges placed at the outer surface of the cylinder that typically is made of steel. The material properties of the steel cylinder are assumed to be known in advance.

Three different conceptual problems arise when the unilateral compression is applied by using the GREAC cell. First, measuring the axial strain, axial stress and radial stress in the unknown material does not mean that only one unique constitutive model can be constructed from the data. The reason for this is partly due to geometry and partly due to the flexibility of material models. Second, boundary effects come into play due to the finite length of a cylinder and that the cylinder is longer than the test specimen due to the rather large compression of powder type materials. This typically means the outer (and inner) surface of the hollow cylinder tends to expand outwards in the region where the test sample is in contact with the cylinder. A question then is what equations that can be used to find the radial stress at the inner surface as a function of the strains (that are measured) at the outer surface. Third, due to friction between the test sample and the hollow cylinder along the inner wall, the GREAC cell will not show a purely unilateral compression situation. In principle this invalids the whole test, but ways to handle the problem is analyzed in this report. The theoretical solution accounts for large strain in some respect. See also reference [1] for further details.

2 The experimental setup in the GREAC cell

The basic setup of the unilateral compression/compaction test is shown in figure 2.1

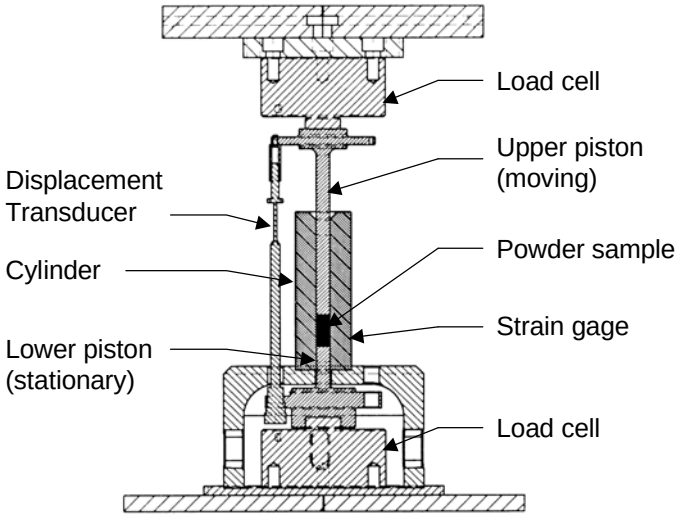

Figure 2.1: The apparatus used in the unilateral compression experiments.

The forces on both the upper and the lower pistons are recorded, but only the upper piston moves relative to the cylinder. The strain gauges measure both the axial strain and the circumferential strain (hoop strain) at the outer surface of the steel cylinder. The displacement transducer measures the volumetric change (axial displacement) of the test material. The radial expansion of the test material along the inner surface can to a good approximation be neglected when calculating the volumetric change of the material.

We apply four basic assumptions concerning the symmetry and setup

$$\sigma_{rz} \overset{mod}{=} 0,\ \frac{\partial \sigma_r}{\partial r} \overset{mod}{=} 0,\ u_r \overset{mod}{=} 0,\ u_z \overset{mod}{=} u_z(z) \tag{2.1}$$

where "mod" means model assumption. σ_r is the radial stress and σ_{rz} is the shear stress. u_z and u_r is the axial and radial displacement of the test sample. All quantities in this section are for the test material.

The equation of motion for a quasi-static situation and the definitions of logarithmic strains then gives

$$\sigma_r = \sigma_\theta,\ \varepsilon_\theta \overset{def}{=} -Ln\left(1-u_r/r\right) = 0,\ \varepsilon_r \overset{def}{=} -Ln\left(1-\partial u_r/\partial r\right) = 0 \tag{2.2}$$

σ_θ is the circumferential stress. The stresses are then

$$
\begin{aligned}
&p \overset{def}{=} -\frac{1}{3}\left(\sigma_r+\sigma_\theta+\sigma_z\right)=-\frac{1}{3}\left(2\sigma_r+\sigma_z\right),\\
&s_z \overset{def}{=} \sigma_z-\frac{1}{3}\left(\sigma_z+\sigma_r+\sigma_\theta\right),\ s_r \overset{def}{=} \sigma_r-\frac{1}{3}\left(\sigma_z+\sigma_r+\sigma_\theta\right)=s_\theta,\\
&s_z+s_r+s_\theta=s_z+2s_r=0,\\
&\sigma_{eff} \overset{def}{=} \left(\frac{3}{2}s_{ij}{}^2\right)^{1/2}=\left(\frac{3}{2}\left(s_z{}^2+s_\theta{}^2+s_r{}^2\right)\right)^{1/2}=\frac{3}{2}\left|s_z\right|=-\frac{3}{2}s_z=\sigma_r-\sigma_z
\end{aligned}
\tag{2.3}
$$

where "def" means definition. p is called the pressure and σ_z is the axial stress. s_r, s_z and s_θ are called the deviatoric stresses while σ_{eff} is called the effective stress or von Mises stress. During compression of the confined sample in the GREAC cell the signs of the stresses are $\sigma_z \le 0,\ s_z \le 0,\ \sigma_r \le 0,\ s_r \ge 0$ and $p \ge 0$. The reason is that most materials tend to expand radially when compressed axially. This means that the axial stress and the radial stress should have the same sign since the cylindrical walls prevent the sample material from expanding radially when the compressive stress is applied axially. Since both the axial and the radial stress are negative it follows that the pressure is positive, the axial deviatoric stress is negative while the radial deviatoric stress is positive.

Moreover, the reduced strains e_z, e_r, e_θ and the effective strain e_{eff} are according to the definitions in the literature given by

$$
\begin{aligned}
&e_z \overset{def}{=} \varepsilon_z-(1/3)\left(\varepsilon_z+\varepsilon_\theta+\varepsilon_r\right)=\frac{2}{3}\varepsilon_z,\ e_r \overset{def}{=} \varepsilon_r-(1/3)\left(\varepsilon_z+\varepsilon_\theta+\varepsilon_r\right)=-\frac{1}{3}\varepsilon_z=-\frac{1}{2}e_z,\ e_\theta=e_r,\\
&e_{eff} \overset{def}{=} \left(\frac{2}{3}e_{ij}{}^2\right)^{1/2}=\left(\frac{2}{3}\left(e_r{}^2+e_\theta{}^2+e_z{}^2\right)\right)^{1/2}=-e_z,
\end{aligned}
\tag{2.4}
$$

The density is given by the mass conservation equation, to read

$$
\begin{aligned}
&A_0\rho_0 dz_0 \overset{mod}{=} A\rho dz \Rightarrow \frac{\partial}{\partial z}\left(z-u\right)=\frac{\rho}{\rho_0}\Rightarrow \rho=\rho_0\left(1-\frac{\partial u}{\partial z}\right),\\
&z \overset{mod}{=} z_0+u_z(z,t),\ A \overset{mod}{=} A_0
\end{aligned}
\tag{2.5}
$$

where u_z is the displacement in the axial direction, the subscript "0" denotes the Lagrangian coordinate. A is the cross section area of the test material which we assume is constant and equal to the initial cross section (Lagrangian cross section).

In addition, the logarithmic axial strains is given by

$$
\varepsilon_z \overset{def}{=} -Ln\left(1-\partial u_z/\partial z\right)\Rightarrow \rho=\rho_0\left(1-\frac{\partial u_z}{\partial z}\right)=\rho_0 Exp\left(-\varepsilon_z\right),\ \varepsilon_z=-Ln\left(\frac{\rho}{\rho_0}\right) \tag{2.6}
$$

The quasi steady axial velocity now becomes according to the definition

$$v \overset{def}{=} \frac{\partial u_z}{\partial t} + v\frac{\partial u_z}{\partial z} \Rightarrow v = \frac{\partial u_z / \partial t}{1 - \partial u_z / \partial z} \tag{2.7}$$

It is easy to show that the total derivative of the axial logarithmic strain becomes the velocity gradient, to read

$$\begin{aligned} \frac{d\varepsilon_z}{dt} &= \frac{\partial\left(-Ln\left(1-\partial u_z/\partial z\right)\right)}{\partial t} + v\frac{\partial\left(-Ln\left(1-\partial u_z/\partial z\right)\right)}{\partial z} \\ &= \frac{\partial\left(-Ln\left(1-\partial u_z/\partial z\right)\right)}{\partial t} + \left(\frac{\partial u_z/\partial t}{1-\partial u_z/\partial z}\right)\frac{\partial\left(-Ln\left(1-\partial u_z/\partial z\right)\right)}{\partial z} \\ &= \frac{\partial^2 u_z/\partial z\partial t}{\left(1-\partial u_z/\partial z\right)} + \left(\partial u_z/\partial t\right)\frac{\partial^2 u_z/\partial z^2}{\left(1-\partial u_z/\partial z\right)^2} = \frac{\partial v}{\partial z} \end{aligned} \tag{2.8}$$

Moreover, a typical displacement during the unilateral compression (assuming for this case no wall friction) is

$$\left\{ z \overset{mod}{=} z_0\left(1-\lambda(t)\right),\ z = z_0 + u_z(z,t) \right\} \Rightarrow u_z(z,t) = \frac{-\lambda(t)z}{1-\lambda(t)} \tag{2.9}$$

The axial strain in the test material are then explicitly given by

$$\varepsilon_z = -Ln\left(1-\partial u_z/\partial z\right) = -Ln\left(1+\frac{\lambda(t)}{1-\lambda(t)}\right) = -Ln\left(\frac{1}{1-\lambda(t)}\right) = Ln\left(1-\lambda(t)\right) \tag{2.10}$$

The velocity then becomes

$$v = \frac{\partial u_z/\partial t}{1-\partial u_z/\partial z} = \frac{\dfrac{-\dot{\lambda}(t)z}{1-\lambda(t)} - \dfrac{\lambda(t)z\dot{\lambda}(t)}{\left(1-\lambda(t)\right)^2}}{1+\dfrac{\lambda(t)}{1-\lambda(t)}} = \frac{\dot{\lambda}(t)z}{1-\lambda(t)} \tag{2.11}$$

The density becomes

$$\rho = \rho_0\left(1-\frac{\partial u_z}{\partial z}\right) = \rho_0\left(1-\frac{u_z}{z}\right) = \rho_0\left(1+\frac{\lambda(t)}{1-\lambda(t)}\right) = \rho_0\left(\frac{1}{1-\lambda(t)}\right) \tag{2.12}$$

3 The Mises materials

Many materials can be called Mises materials. This means that one can write

$$\sigma_{eff} = \sigma_{eff}\left(p, e_{eff}\right).$$

Consider first a purely elastic Hook material as a test material, to read from the definitions in the literature

$$\begin{aligned}
&\sigma_z = \frac{E(1-\nu)\varepsilon_z}{(1+\nu)(1-2\nu)},\ \sigma_r = \frac{E\nu\varepsilon_z}{(1+\nu)(1-2\nu)},\ (a)\\
&\sigma_{eff} = -\frac{3}{2}s_z = -\frac{E\varepsilon_z}{(1+\nu)} = -2G\varepsilon_z = -3Ge_z = 3Ge_{eff},\ (b)
\end{aligned} \tag{3.1}$$

The relation in (3.1b) follows easily from the general relation for an elastic Hook material, to read in tensor notation

$$\begin{aligned}
&\sigma_{ij} \overset{mod}{=} \lambda\,\varepsilon_{ll}\delta_{ij} + 2G\varepsilon_{ij} = \underbrace{K\varepsilon_{ll}}_{-p}\delta_{ij} + \underbrace{2G\left(\varepsilon_{ij} - \frac{1}{3}\delta_{ij}\varepsilon_{ll}\right)}_{s_{ij}} =,\ \lambda \overset{def}{=} K - \frac{2}{3}G\\
&\Rightarrow p = -\frac{1}{3}\sigma_{ii}, s_{ii} = 0, s_{ij} = 2Ge_{ij}
\end{aligned} \tag{3.2}$$

Then it follows directly that

$$\begin{aligned}
&\sigma_z = \sigma_{11} = K\left(\varepsilon_{11}+\varepsilon_{22}+\varepsilon_{33}\right) + 2G\left(\varepsilon_{11} - \frac{1}{3}\left(\varepsilon_{11}+\varepsilon_{22}+\varepsilon_{33}\right)\right) = K\varepsilon_{11} + \frac{4}{3}G\varepsilon_{11} = \left(K + \frac{4}{3}G\right)\varepsilon_z\\
&s_z = s_{11} = \frac{4}{3}G\varepsilon_z\\
&\sigma_r = \sigma_{22} = K\left(\varepsilon_{11}+\varepsilon_{22}+\varepsilon_{33}\right) + 2G\left(\varepsilon_{22} - \frac{1}{3}\left(\varepsilon_{11}+\varepsilon_{22}+\varepsilon_{33}\right)\right) = K\varepsilon_{11} - \frac{2}{3}G\varepsilon_{11} = \left(K - \frac{2}{3}G\right)\varepsilon_z\\
&s_r = s_\theta = -\frac{2}{3}G\varepsilon_z,\ p = -K\varepsilon_z
\end{aligned} \tag{3.3}$$

Most materials tend to expand radially when compressed axially. This means that the axial stress and the radial stress should have the same sign since the radial stress prevents the material from expanding radially. This means according to equation (3.3) that $K - \frac{2}{3}G \geq 0 \Rightarrow G \leq \frac{3}{2}K$. The Poisson's ratio is defined by $\nu = \left(3K - 2G\right)/\left(6K + 2G\right)$. Thus the criterion gives that the Poisson's ratio is positive. In addition when the material is compressed axially, the radial stress necessary to constrain the radial expansion is for most materials less or equal to the axial stress.

Thus $\left(K+\frac{4}{3}G\right)\varepsilon_z \geq \left(K-\frac{2}{3}G\right)\varepsilon_z \Rightarrow G \geq 0$. This means that the Poisson's ratio always is less than ½.

For an ideal rigid elastic-plastic Mises material during pure loading (no unloading) we have

$$\begin{aligned}
&\sigma_{eff}^{mod} = 3Ge_{eff} \text{ when } e_{eff} \leq \frac{Y}{3G}, \text{ Elastic, (a)} \\
&\sigma_{eff}^{mod} = Y \text{ when } e_{eff} \geq \frac{Y}{3G}, \text{ Plastic, (b)}
\end{aligned} \tag{3.4}$$

Thus at the onset of plastic flow we achieve

$$3Ge_{eff} = -2G\varepsilon_z = Y \Rightarrow \varepsilon_z = -\frac{Y}{2G} \tag{3.5}$$

The critical stresses at the onset of plastic flow are denoted with the superscript "c". Thus

$$\begin{aligned}
&\sigma_z^c = \left(K+\frac{4}{3}G\right)\varepsilon_z = -\left(K+\frac{4}{3}G\right)\frac{Y}{2G} = -\frac{KY}{2G}-\frac{2}{3}Y,\ s_z = \frac{4}{3}G\varepsilon_z = -\frac{2}{3}Y, \\
&\sigma_r^c = \left(K-\frac{2}{3}G\right)\varepsilon_z = -\frac{KY}{2G}+\frac{Y}{3} = -\left(\frac{3K-2G}{6G}\right)Y,\ s_r = s_\theta = -\frac{2}{3}G\varepsilon_z = \frac{Y}{3}, \\
&p^c = -K\varepsilon_z = \frac{KY}{2G}
\end{aligned} \tag{3.6}$$

During plastic flow (3.4b) applies, i.e. $\sigma_{eff} = Y$. Thus we achieve

$$\begin{aligned}
&\sigma_{eff} = -\frac{3}{2}s_z = Y \\
&\Rightarrow \left\{ s_z = -\frac{2}{3}Y,\ s_r = s_\theta = \frac{Y}{3},\ \sigma_z = K\varepsilon_z - \frac{2}{3}Y,\ \sigma_r = \sigma_\theta = K\varepsilon_z + \frac{Y}{3},\ \sigma_r - \sigma_z = Y,\ p = -K\varepsilon_z \right\}
\end{aligned} \tag{3.7}$$

Consider now the more general test model, to read

$$\sigma_{eff}^{mod} = Y\left(1 - Exp\left(-e_{eff}\,3G/Y\right)\right),\ Y = const.,\ G = const.,\ p = -K\left(\varepsilon_{ll}\right)\varepsilon_{ll} \tag{3.8}$$

where Y is the ultimate stress, and G is a shear modulus. During unilateral compression we achieve that

$$\begin{aligned}
&\sigma_{eff}\left(e_{eff}\right) = \sigma_r - \sigma_z = Y\left(1 - Exp\left(-e_{eff}\,3G/Y\right)\right) \\
&= Y\left(1 - Exp\left(2\varepsilon_z G/Y\right)\right),\ Y = const.,\ G = const.,\ p = -K\left(\varepsilon_z\right)\varepsilon_z
\end{aligned} \tag{3.9}$$

Thus by plotting the stress difference $\sigma_r - \sigma_z$ against ε_z one can reveal G and Y. By plotting $p = -\frac{1}{3}(2\sigma_r + \sigma_z)$ against ε_z one can reveal $K(\varepsilon_z)\varepsilon_z$. Any form $\sigma_{eff} = \sigma_{eff}(e_{eff})$ can be used.

Consider the model $\sigma_{eff} = \sigma_{eff}(p)$. This is a typical model for granular materials. The yield stress is accordingly not a function of the strain (as for steel materials) but a function of the pressure. This functionality can be revealed by plotting $\sigma_{eff}(p) = \sigma_r - \sigma_z$ against $p = -\frac{1}{3}(\sigma_r + \sigma_\theta + \sigma_z) = -\frac{1}{3}(2\sigma_r + \sigma_z)$.

Finally consider $\sigma_{eff} = \sigma_{eff}(p, e_{eff})$. We achieve that

$$\sigma_r - \sigma_z = \sigma_{eff}(p, e_{eff}) = \sigma_{eff}\left(-\frac{1}{3}(2\sigma_r + \sigma_z), -\frac{2}{3}\varepsilon_z\right) \tag{3.10}$$

In section 9 we outline the model for cyclic loading and unloading.

4 Calculation of the radial stress assuming no shear stresses

As mentioned in the introduction the radial stress of the unknown test material is not readily measured. Typically one calculates this quantity by measuring the axial and circumferential strain at the outer surface of a well known casing cylinder. The cylinder is typically made of steel or wolfram. Note that in this section we consider only stresses and strains in the casing material. Thus for simplicity we choose the same mathematical symbols as in the last section for the test material inside the hollow cylinder.

When radial and axial stresses apply at the inner surface of a steel cylinder the cylinder expands and deforms radially and axially. As a fundamental approximation for the casing cylinder the following displacements applies

$$u_r \overset{mod}{=} u_r(r),\ u_z \overset{mod}{=} u_z(z) \tag{4.1}$$

It is assumed that the material model for the casing cylinder is well known. Say, a material that follows Hooke's law, to read

$$\begin{aligned}
\sigma_z &= \frac{E}{(1+\nu)(1-2\nu)}\left((1-\nu)\varepsilon_z + \nu(\varepsilon_\theta + \varepsilon_r)\right),\\
\sigma_r &= \frac{E}{(1+\nu)(1-2\nu)}\left((1-\nu)\varepsilon_r + \nu(\varepsilon_\theta + \varepsilon_z)\right),\\
\sigma_\theta &= \frac{E}{(1+\nu)(1-2\nu)}\left((1-\nu)\varepsilon_\theta + \nu(\varepsilon_r + \varepsilon_z)\right),
\end{aligned} \tag{4.2}$$

The logarithmic strains in the steel cylinder are according to the definition

$$\varepsilon_z = -Ln\left(1-\partial u_z/\partial z\right), \varepsilon_r = -Ln\left(1-\partial u_r/\partial r\right), \varepsilon_\theta = -Ln\left(1-u_r/r\right) \tag{4.3}$$

The equation of motion is when neglecting shear stresses (which follows when using equation (4.1))

$$\frac{\partial \sigma_r}{\partial r} + \frac{\sigma_r - \sigma_\theta}{r} = 0 \tag{4.4}$$

Inserting the stresses in equation (4.2) into equation (4.4) gives directly that

$$\frac{\partial\left((1-\nu)\varepsilon_r + \nu\,\varepsilon_\theta\right)}{\partial r} + \frac{(1-2\nu)\left(\varepsilon_r - \varepsilon_\theta\right)}{r} = 0 \tag{4.5}$$

Mass conservation now gives for the logarithmic strains

$$\left(1-\partial u_z/\partial z\right)\left(1-\partial u_r/\partial r\right)\left(1-u_r/r\right) = \frac{\rho_0}{\rho} \Rightarrow \varepsilon_z + \varepsilon_r + \varepsilon_\theta = -Ln\left(\frac{\rho}{\rho_0}\right) \tag{4.6}$$

where the axial strain ε_z is independent of the radial position due to the relation in equation (4.1). It then follows from (4.6) that

$$\frac{\partial\left(\varepsilon_r + \varepsilon_\theta\right)}{\partial r} = -\frac{\partial}{\partial r}\left(Ln\left(\frac{\rho}{\rho_0}\right)\right) = \frac{1}{\rho}\frac{\partial \rho}{\partial r} \tag{4.7}$$

We apply the ad hoc approximation

$$\frac{\partial \rho}{\partial r} \approx 0 \tag{4.8}$$

which can in fact be proven to be exact for small strains due to the relation $\partial\varepsilon_\theta/\partial r = \left(\varepsilon_r - \varepsilon_\theta\right)/r$, valid for small strains[1]. Thus we achieve from equation (4.7) and equation (4.8) that $\partial\left(\varepsilon_r + \varepsilon_\theta\right)/\partial r = 0$. Together with equation (4.5) we have two equations, to read after a simple mathematical reorganization

$$\frac{\partial \varepsilon_\theta}{\partial r} + \frac{\partial \varepsilon_r}{\partial r} = 0, \frac{\partial \varepsilon_r}{\partial r} + \frac{\varepsilon_r - \varepsilon_\theta}{r} = 0 \tag{4.9}$$

[1] $\partial\varepsilon_\theta/\partial r = \left(\varepsilon_r - \varepsilon_\theta\right)/r$, $\partial\left((1-\nu)\varepsilon_r + \nu\,\varepsilon_\theta\right)/\partial r + (1-2\nu)\left(\varepsilon_r - \varepsilon_\theta\right)/r = 0$ gives that $\partial\left(\varepsilon_r + \varepsilon_\theta\right)/\partial r = 0$.

The solution of the first equation is given by $\varepsilon_\theta = -\varepsilon_r + 2a$, where a is a constant. Inserting the second equation into (4.9) gives $\partial\varepsilon_r / \partial r = -2\varepsilon_r / r + 2a / r \Rightarrow \varepsilon_r = a - b / r^2$, where b is a new constant. Thus we achieve the solution

$$\varepsilon_r = a - \frac{b}{r^2},\ \varepsilon_\theta = a + \frac{b}{r^2} \tag{4.10}$$

In addition we achieve the radial stress when inserting equation (4.10) into equation (4.2), to read

$$\sigma_r = \frac{E}{(1+\nu)(1-2\nu)}\left((1-\nu)\varepsilon_r + \nu(\varepsilon_\theta + \varepsilon_z)\right) = \frac{E}{(1+\nu)(1-2\nu)}\left(a - (1-2\nu)\frac{b}{r^2} + \nu\varepsilon_z\right) \tag{4.11}$$

The radial displacement is given by the definition in equation (4.3) and equation (4.10), to read

$$\begin{aligned} &\varepsilon_\theta = a + \frac{b}{r^2} = -Ln\left(1 - u_r / r\right) \Rightarrow u_r = r\left(1 - Exp\left(-a - \frac{b}{r^2}\right)\right), \text{ (a)} \\ &r_0 = r - u_r = r\,Exp\left(-a - \frac{b}{r^2}\right), \text{ (b)} \end{aligned} \tag{4.12}$$

where r_0 is the Lagrangian radial coordinate.

Let R_1 and R_2 denote the Lagrangian radial coordinate of the inner and outer surface of the steel cylinder respectively. Equation (4.12) gives the relations

$$\begin{aligned} &r_0 = R_1 \Rightarrow R_1 = r\,Exp\left(-a - \frac{b}{r^2}\right) = r^E\left(a,b,r\right) \Rightarrow r = r^{-E}\left(a,b,R_1\right) \\ &r_0 = R_2 \Rightarrow R_2 = r\,Exp\left(-a - \frac{b}{r^2}\right) = r^E\left(a,b,r\right) \Rightarrow r = r^{-E}\left(a,b,R_2\right) \\ &r^E\left(a,b,r\right) \overset{def}{=} r\,Exp\left(-a - \frac{b}{r^2}\right) = Exp\left(-a\right)\frac{r}{Exp\left(b / r^2\right)} \end{aligned} \tag{4.13}$$

The function r^E is invertible in r and the inverse function r^{-E} can be found. To simplify the notation we write $r_1 = r^{-E}\left(a,b,R_1\right)$ as $R(a,b,R_1)$ and $r_2 = r^{-E}\left(a,b,R_2\right)$ as $R(a,b,R_2)$.

We can develop analytical formulas to first, second and third order, to read

$$R(a,b,R_1) = R_1, \text{ (first)},$$
$$R(a,b,R_1) = R_1\, Exp\left(a + b/{R_1}^2\right), \text{ (second)} \tag{4.14}$$
$$R(a,b,R_1) = R_1\, Exp\left(a + \frac{b}{{R_1}^2\, Exp\left(2a + 2b/{R_1}^2\right)}\right), \text{ (third)}$$

Analogously for the outer boundary.

Moreover, the boundary conditions at the inner and outer surface of the steel cylinder is given as

$$\sigma_r = -\overline{p}, \text{ when } r = R(a,b,R_1), \sigma_r = 0, \text{when } r = R(a,b,R_2) \tag{4.15}$$

where we denote the radial stress in the test material at the inner surface of the cylinder as $-\overline{p}$ in this section. Equation (4.10), (4.11) and the boundary condition in equation (4.15) gives

$$\begin{aligned}
\sigma_r\left(r = R(a,b,R_1),\right) &= \frac{E}{(1+\nu)(1-2\nu)}\left(a - (1-2\nu)\frac{b}{R(a,b,R_1)^2} + \nu\,\varepsilon_z\right) = -\overline{p} \\
\sigma_r\left(r = R(a,b,R_2)\right) &= \frac{E}{(1+\nu)(1-2\nu)}\left(a - (1-2\nu)\frac{b}{R(a,b,R_2)^2} + \nu\,\varepsilon_z\right) = 0
\end{aligned} \tag{4.16}$$

The "solution" is

$$\begin{aligned}
a &= \frac{\overline{p}R(a,b,R_1)^2}{R(a,b,R_2)^2 - R(a,b,R_1)^2}\frac{(1+\nu)(1-2\nu)}{E} - \nu\,\varepsilon_z, \\
b &= \frac{\overline{p}R(a,b,R_1)^2 R(a,b,R_2)^2}{R(a,b,R_2)^2 - R(a,b,R_1)^2}\frac{(1+\nu)}{E}
\end{aligned} \tag{4.17}$$

Notice that ε_z is independent of the radial coordinate *r* due to equation (4.1). In equation (4.17) the dependency of *a* and *b* is on both sides of the equality sign when using the second and third order solution in equation (4.14). In general only numerical solutions are achievable for an "exact" solution. The solution of equation (4.17) can be written as $a = a\left(R_1, R_2, \overline{p}\right)$ and $b = b\left(R_1, R_2, \overline{p}\right)$. This solution can be used to establish the Eulerian coordinate of the inner and outer surface of the cylinder as a function of the Lagrangian coordinate, to read

$$r_1 = R\left(a\left(R_1,R_2,\overline{p}\right), b\left(R_1,R_2,\overline{p}\right), R_1\right),\ r_2 = R\left(a\left(R_1,R_2,\overline{p}\right), b\left(R_1,R_2,\overline{p}\right), R_2\right) \tag{4.18}$$

The circumferential strain ε_θ at the outer boundary $r = r_2$ is usually measured. It is given theoretically from equation (4.10), by using equation (4.17), to read

$$\varepsilon_\theta(r=r_2)=a+\frac{b}{{r_2}^2}=\frac{\overline{p}\,{r_1}^2}{{r_2}^2-{r_1}^2}\frac{(1+\nu)(1-2\nu)}{E}-\nu\,\varepsilon_z+\frac{\overline{p}\,{r_1}^2}{{r_2}^2-{r_1}^2}\frac{(1+\nu)}{E}=\frac{\overline{p}\,{r_1}^2 2(1-\nu^2)}{\left({r_2}^2-{r_1}^2\right)E}-\nu\,\varepsilon_z \tag{4.19}$$

It follows directly from equation (4.19) after some algebraic manipulations that the radial stress at the inner surface of the cylinder is

$$\sigma_r(r=r_1)=-\overline{p}=-\frac{E}{2(1-\nu^2)}\left({r_2}^2/{r_1}^2-1\right)\left(\varepsilon_\theta(r=r_2)+\nu\,\varepsilon_z\right) \tag{4.20}$$

where r_1 and r_2 are given in equation (4.18). Notice that if r_1, r_2, $\varepsilon_\theta(r=r_2)$ and $\varepsilon_z(r=r_2)$ are measured, equation (4.20) can be used directly to find the inner radial stress $-\overline{p}$. Only a numerical solution is achievable if r_1 and r_2 are not measured (by equation (4.18)). But we will find good approximations without measuring r_1 or r_2.

The axial stress can be found. Using equation (4.11) and the boundary condition that the radial stress is zero at the outer surface of the cylinder gives

$$\begin{aligned}&\sigma_r=\frac{E}{(1+\nu)(1-2\nu)}\left((1-\nu)\varepsilon_r+\nu(\varepsilon_\theta+\varepsilon_z)\right),\\&\sigma_r\left(r=r_2\right)=0\Rightarrow\varepsilon_r\left(r=r_2\right)=\frac{-\nu\left(\varepsilon_\theta\left(r=r_2\right)+\varepsilon_z\right)}{(1-\nu)}\end{aligned} \tag{4.21}$$

The axial stress at the outer surface then becomes when using equations (4.2) and (4.21)

$$\sigma_z=\frac{E}{(1+\nu)(1-2\nu)}\left((1-\nu)\varepsilon_z+\nu(\varepsilon_\theta+\varepsilon_r)\right)=\frac{E}{(1-\nu^2)}\left(\varepsilon_z+\nu\,\varepsilon_\theta(r=r_2)\right) \tag{4.22}$$

Notice that the axial stress is independent of the radial coordinate since $\partial\left(\varepsilon_\theta+\varepsilon_r\right)/\partial r=\partial\varepsilon_z/\partial r=0$ according to equation (4.1), (4.9) and the definition in equation (4.3).

If for some reason the axial stress is zero, it follows from (4.22) that $\varepsilon_z=-\nu\,\varepsilon_\theta(r=r_2)$. Inserting into the general equation (4.20) gives the well known formulae

$$\overline{p}=\frac{E}{2}\left({r_2}^2/{r_1}^2-1\right)\varepsilon_\theta(r=r_2) \tag{4.23}$$

Where r_1 and r_2 are given in equation (4.18).

The lowest order solution is typically a very good approximation. We achieve to lowest order the solution

$$\sigma_r(r=r_1) = -\overline{p},$$

$$\overline{p} \approx \frac{E}{2(1-\nu^2)}\left({R_2}^2/{R_1}^2 - 1\right)\left(\varepsilon_\theta(r=r_2) + \nu\,\varepsilon_z(r=r_2)\right),$$

$$\overline{p} \approx \frac{E}{2}\left({R_2}^2/{R_1}^2 - 1\right)\varepsilon_\theta(r=r_2), \text{ when } \varepsilon_z(r=r_2) = -\nu\,\varepsilon_\theta(r=r_2)$$

$$\sigma_z = \frac{E}{1-\nu^2}\left(\varepsilon_z(r=r_2) + \nu\,\varepsilon_\theta(r=r_2)\right) \tag{4.24}$$

$$r_1 \approx R_1 + aR_1 + \frac{b}{R_1} = R_1 + \frac{\overline{p}{R_1}^2}{{R_2}^2 - {R_1}^2}\frac{(1+\nu)(1-2\nu)}{E}R_1 + \frac{\overline{p}R_1{R_2}^2}{{R_2}^2 - {R_1}^2}\frac{(1+\nu)}{E}$$

$$= R_1 + \frac{\overline{p}(1+\nu)}{E\left({R_2}^2 - {R_1}^2\right)}\left({R_1}^2(1-2\nu) + R_1{R_2}^2\right)$$

The material properties of the steel cylinder are given in appendix A.

5 Test of the formula in (4.24) to calculate the radial stress at the inner surface.

The loading apparatus is a long cylinder where the test sample is only occupying a limited region (see figure 2.1). Due to this the steel cylinder tends to bulge somewhat outwards due to the test samples only being in contact with the cylinder in a small region. In principle this invalids the assumption in equation (4.1) since the radial displacement will be dependent of z. Thus we must consider equation (4.1) as an approximation. To test whether the formula in (4.20) still is applicable as an approximation we inserted and tested two well known materials, rubber and aluminum (7075-T6). The Poisson's ratio for rubber is known to be close to 0.5 (0.4998) [2] since the shear modulus, *G*, is much smaller than the bulk modulus, *K*. Rubber materials also show strong nonlinearity as a function of the strain for both moduli. Notice that aluminum has a Poisson's ratio of 0.33.

5.1 Rubber

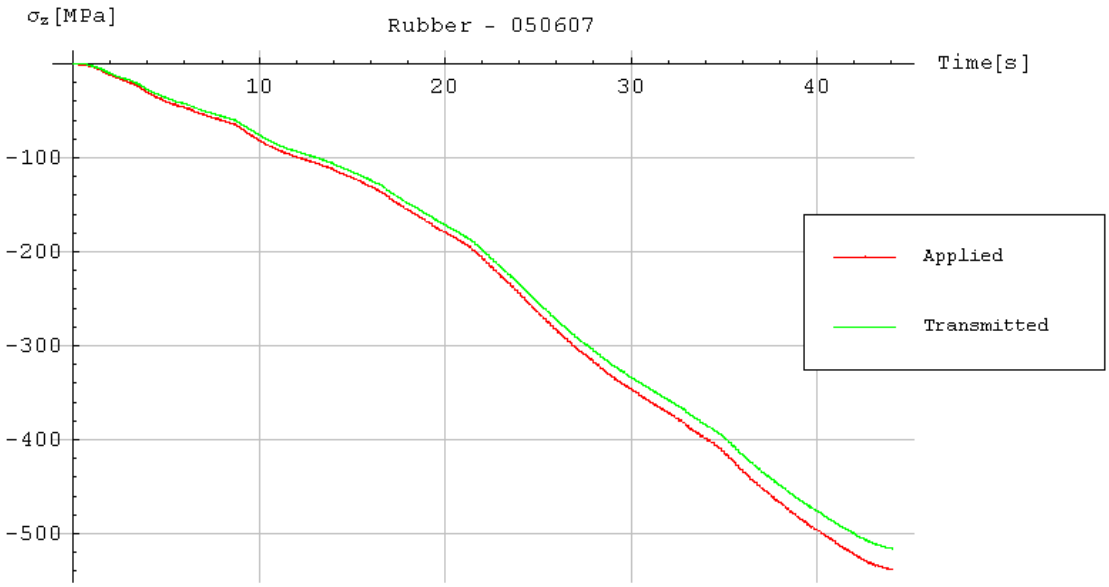

Figure 5.1: The axial stress as a function of time for the upper and lower piston when compressing rubber.

Figure 5.1 shows the axial stress in the test material measured by the upper and lower piston. The stress is given by the force divided by the cross section area of the specimen (given as πR_1^2). The wall friction along the inner surface of the steel cylinder is shown to be small since the upper and lower stresses are almost the same. A tissue paper was used to lower the wall friction.

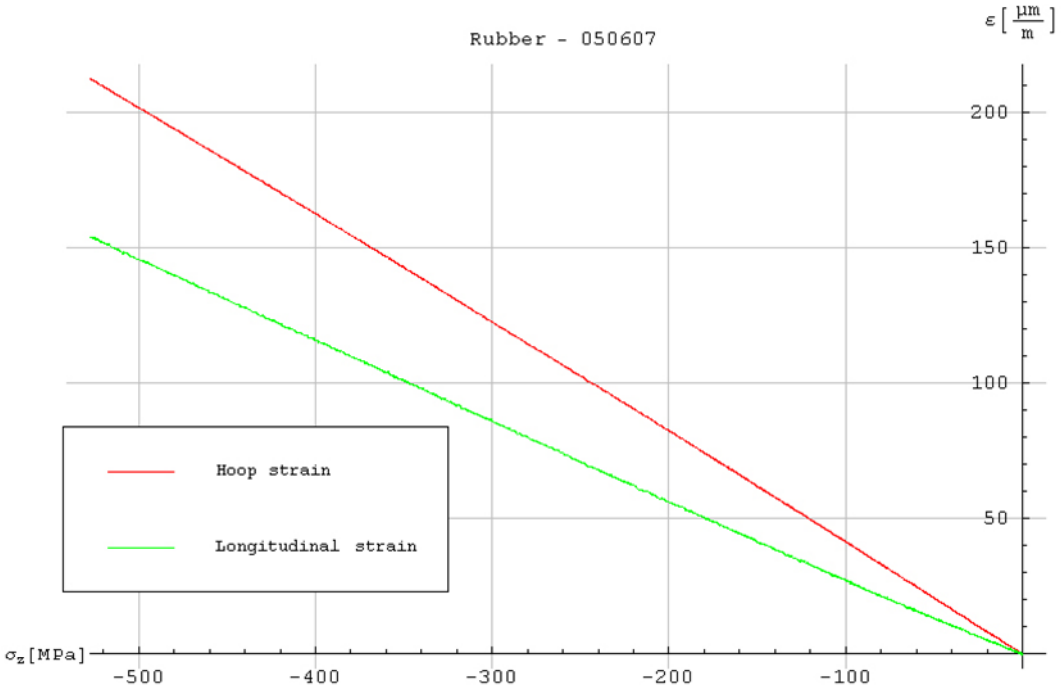

Figure 5.2: The circumferential (hoop) and axial (axial) strain on the outer steel cylinder as a function of the axial stress in the test sample.

Figure 5.2 shows the circumferential and axial strains as a function of the axial stress (average of top and bottom) on the test sample. Notice that the formula $\varepsilon_z = -\nu\,\varepsilon_\theta(r = R_2')$ does not hold at all. Actually the axial and the circumferential (hoop) strain both have the same sign, are of the same magnitude and are positive. Thus the outer surface of the cylinder is in a state of tension (positive stress) both axially and circumferentially. Both the axial and the circumferential strain at the outer surface must be measured and inserted into formula (4.24) to give the radial stress in the test material.

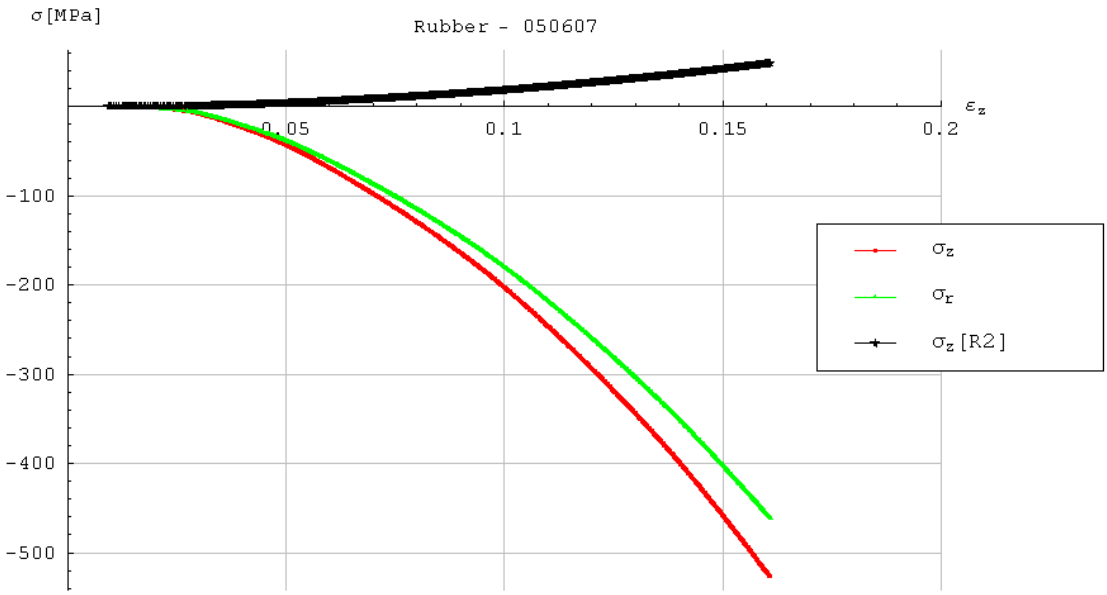

Figure 5.3: Different stresses as a function of axial strain.

Figure 5.3 shows the calculated radial stress and the measured axial stress in the test sample as a function of the axial strain in the test sample. Also shown is the axial stress in the cylinder found by the formula in equation (4.22) (red curve). The two axial stresses are quite unequal with opposite sign. This shows that the axial stress in the steel cylinder is not caused by friction along the walls, but by outward expansion (bulging) of the steel cylinder in the contact region between the sample and the cylinder.

Now, we assume a nonlinear rubber material of the form

$$\sigma_{ij}^{\,mod} = \bar{K}(\varepsilon_{ll})\,\varepsilon_{ll}\delta_{ij} + 2\bar{G}(\varepsilon_{ll})\left(\varepsilon_{ij} - \frac{1}{3}\delta_{ij}\varepsilon_{ll}\right) \tag{5.1}$$

Then it follows that

$$\sigma_z = \left(\bar{K}(\varepsilon_z) + \frac{4}{3}\bar{G}(\varepsilon_z)\right)\varepsilon_z, \qquad \sigma_r = \left(\bar{K}(\varepsilon_z) - \frac{2}{3}\bar{G}(\varepsilon_z)\right)\varepsilon_z \tag{5.2}$$

This gives that

$$k \overset{def}{=} \frac{\sigma_r}{\sigma_z} = \frac{\bar{K}(\varepsilon_z) - \frac{2}{3}\bar{G}(\varepsilon_z)}{\bar{K}(\varepsilon_z) + \frac{4}{3}\bar{G}(\varepsilon_z)} \approx 1 - 2\bar{G}(\varepsilon_z)/\bar{K}(\varepsilon_z), \quad \sigma_r - \sigma_z = -2\bar{G}(\varepsilon_z)\varepsilon_z,$$
$$\nu' = \frac{k}{1+k} = \frac{3\bar{K}(\varepsilon_z) - 2\bar{G}(\varepsilon_z)}{6\bar{K}(\varepsilon_z) + 2\bar{G}(\varepsilon_z)} \approx \frac{1}{2}\left(1 - \bar{G}(\varepsilon_z)/\bar{K}(\varepsilon_z)\right) \tag{5.3}$$

The definition of the bulk modulus, K, shear modulus, G, and the Poisson's ratio are given by

$$K \overset{def}{=} -\frac{\partial p}{\partial \varepsilon_z} = \frac{1}{3}\frac{\partial(\sigma_z + 2\sigma_r)}{\partial \varepsilon_z}, \quad G \overset{def}{=} -\frac{1}{2}\frac{\partial(\sigma_r - \sigma_z)}{\partial \varepsilon_z}$$
$$\nu \overset{def}{=} \frac{3K(\varepsilon_z) - 2G(\varepsilon_z)}{6K(\varepsilon_z) + 2G(\varepsilon_z)} \approx \frac{1}{2}\left(1 - G(\varepsilon_z)/K(\varepsilon_z)\right) \tag{5.4}$$

In general the Poisson's ratio, ν, is not quite equal to the number ν' in equation (5.3).

The bulk modulus and the shear modulus of our sample of rubber were not exactly known and we could only test our mathematical relations by the Poisson's ratio. The material properties of rubber are given in appendix B.

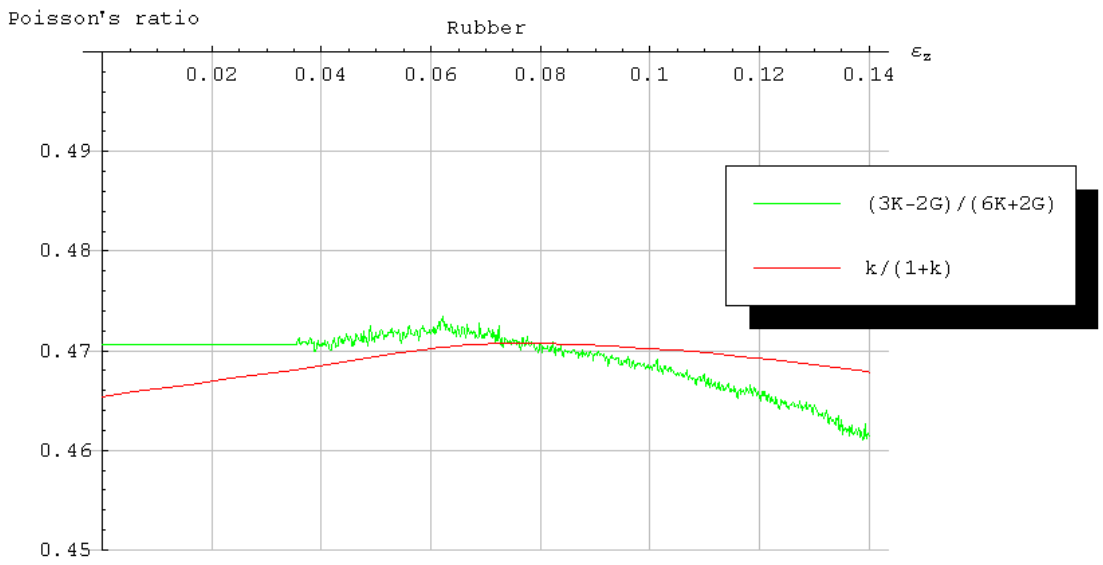

Figure 5.4: The established Poisson's ratio as a function of axial strain in the test sample.

Figure 5.4 shows the results for the Poisson's ratio and the fraction k/(1+k) as a function of the axial strain. We find a value close to 0.47 while the data in appendix B reports 0.4998.

When finding the shear and the bulk modulus we performed a differentiation of the pressure and the von Mises stress in the test sample. To be able to perform this we smoothed the stress-strain curves before differentiation. The smoothing techniques were of the moving average type. The curves in figure 5.4 are the average over 4 different runs of the loading apparatus.

In the next section we discuss the reason for the deviation from 0.4998 which should have been the result, and why the curves in figure 5.4 are not constant.

5.2 Aluminum

A sample of aluminum (7075-T6) was shrink fitted into the GREAC cylinder. This was to ensure that the relatively small elastic deformations of the aluminum would be detectable for the strain gauges at the outer surface of the GREAC cylinder. The inner diameter of the GREAC cylinder was measured to be 17.094 mm. The aluminum sample was made with a diameter of 17.11 mm (and 16.76 mm long). The aluminum sample was then cooled in liquid nitrogen so that the diameter decreased to approximately 17.05 mm and then inserted into the GREAC cylinder.

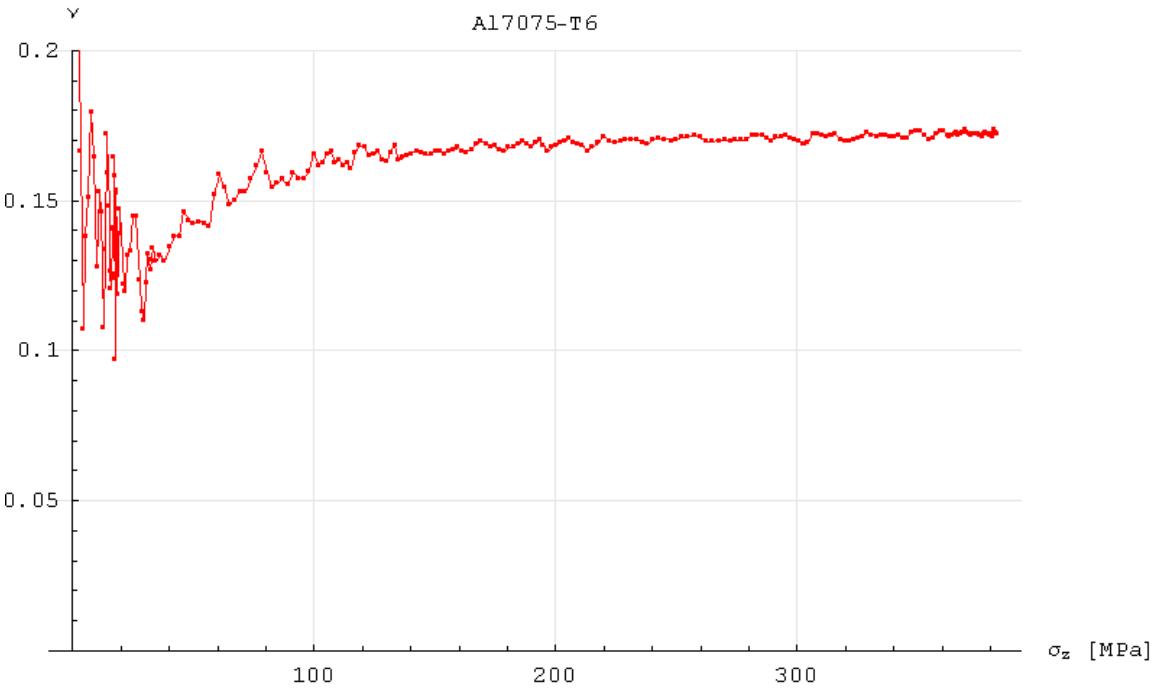

Figure 5.5: Measured Poisson's ratio as a function of axial stress.

As can be seen from figure 5.5 the measured Poisson's ratio does not match with the actual Poisson's ratio of 0.33 for aluminum. This seem to be due to relatively small strains for the aluminum sample since the rubber gives much better agreement with the literature values [2].

6 Robustness tests of strain gauges

The measured strains on the outer surface of the steel cylinder show that the cylinder tends to bulge somewhat outwards due to the tests sample only being in contact with the cylinder in a small region. To test the robustness of our apparatus in relation to the position of the strain gauges we have performed different tests with the rubber test material.

a) The strain gauges are placed on both sides of the cylinder to take in consideration bending (figure 6.1).
b) A strain gauge is displaced somewhat in the axial direction to see the significance of this displacement in relation to the expansion of the cylinder (figure 6.2).

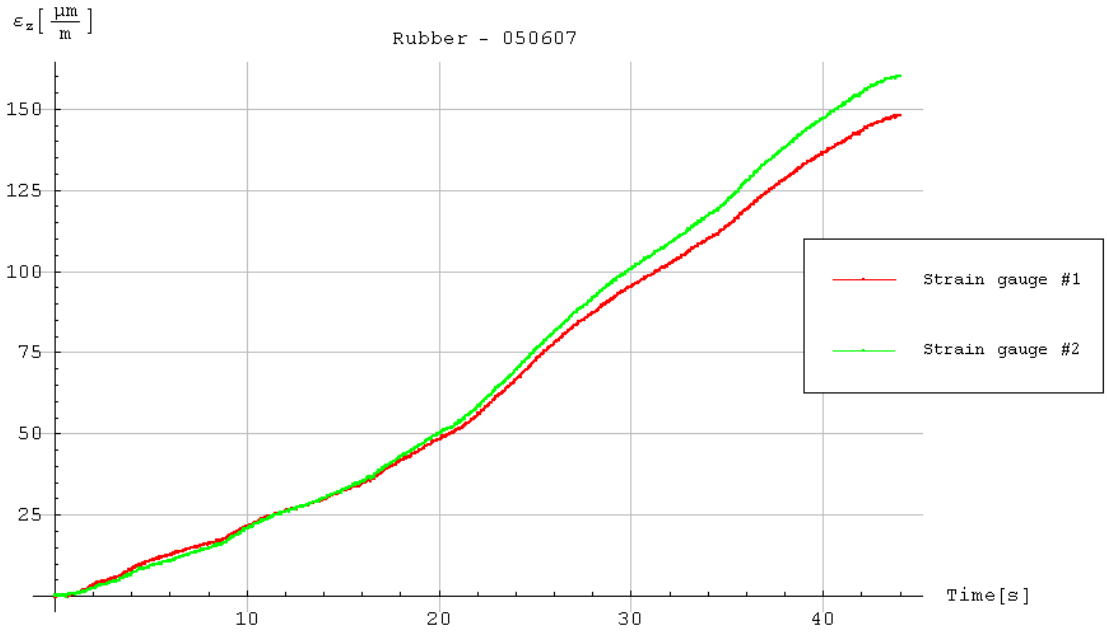

Figure 6.1: Comparison between the axial strain gages on both sides of the cylinder. A slight bending is observed.

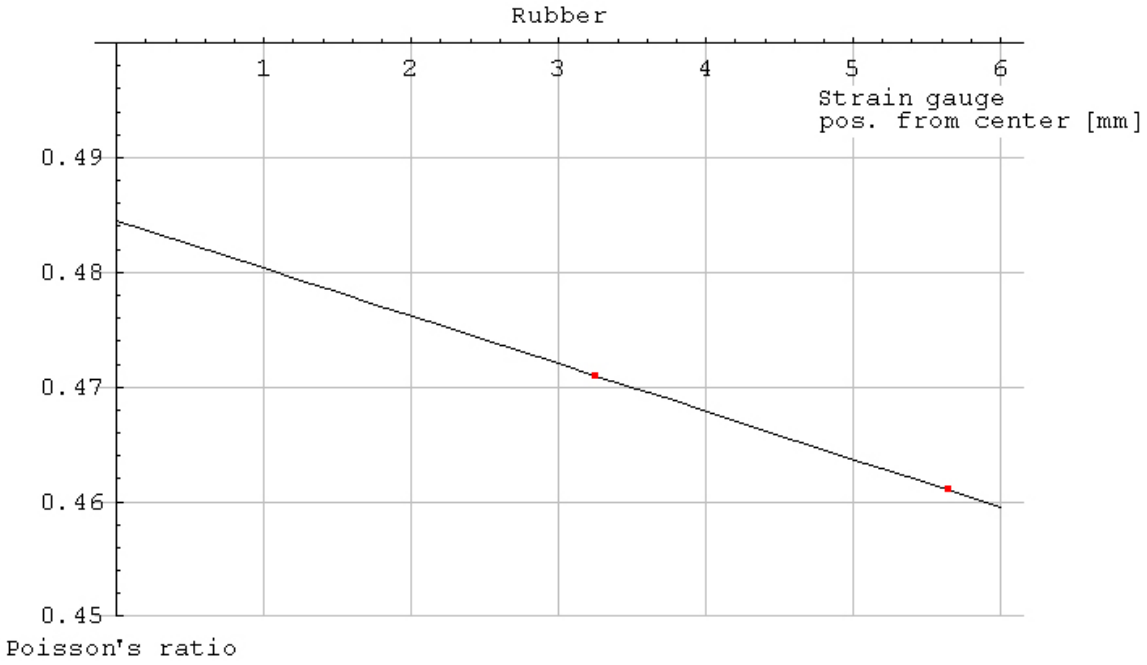

■ Measurements, —— Estimated Poisson's ratio as a function of strain gauge position

Figure 6.2: Maximum Poisson's ratio vs. strain gauge position relative to center of sample at maximum compression.

In figure 6.1 we find a small difference between the axial strains on the opposite sides of the cylinder. This shows a small bending, but it is not significant. For every run with a material one has to check that the two gauges give approximately the same values.

Looking at figure 5.4 we find that the Poisson's ratio is varying with the axial strain. The literature does not report that the Poisson's ratio is varying. In addition our maximum value of the Poisson's ratio is somewhat too low. It should have been closer to 0.5. We believe that the reason for the discrepancies is mainly that the strain gauges are off the middle point of the test sample. But for our chosen positions of the gauges they are really coming closer to the middle point when the load increases. Figure 6.2 show the maximum estimated Poisson's ratio as a function of the strain gauges position off the middle point of the test sample. By extrapolating the curve back to zero deviation (i.e. at the middle point) we find that the Poisson's ratio becomes larger. It turns out that to achieve good material data the clue is to position the strain gauges at the outer cylinder surface at the middle point of the sample. But during a test this point is varying and is not a fixed position on the steel cylinder. Thus in principle we must change the position of the gauges (since they are few) during a test, or we could consider a test to be valid only at one load, i.e., the load where the gauges are at the middle point of the test sample.

7 Robustness tests of the axial displacement of the piston

The axial displacement of the granular material is important for establishing a constitutive model. During compression the pistons made of hardened steel will be compressed in the axial direction.

From figure 2.1 it can be seen that this compression must be subtracted from the reading of the displacement transducers to reach the true compression of the test material. Appendix C gives the material properties of the piston. The upper and lower pistons are during compression in a state of simple compression. Thus the displacement Δu of the pistons is found by

$$\sigma_z = E\varepsilon_z \approx E\frac{\Delta u}{l_0} \Rightarrow \Delta u \approx \frac{\sigma_z}{E} l_0 \tag{7.1}$$

l_0 = total length of the two pistons, Δu = displacement to be subtracted

To check this formula a test was performed without any test material. We simply compress the two pistons against each other. Figure 7.1 shows the results together with the formula in equation (7.1).

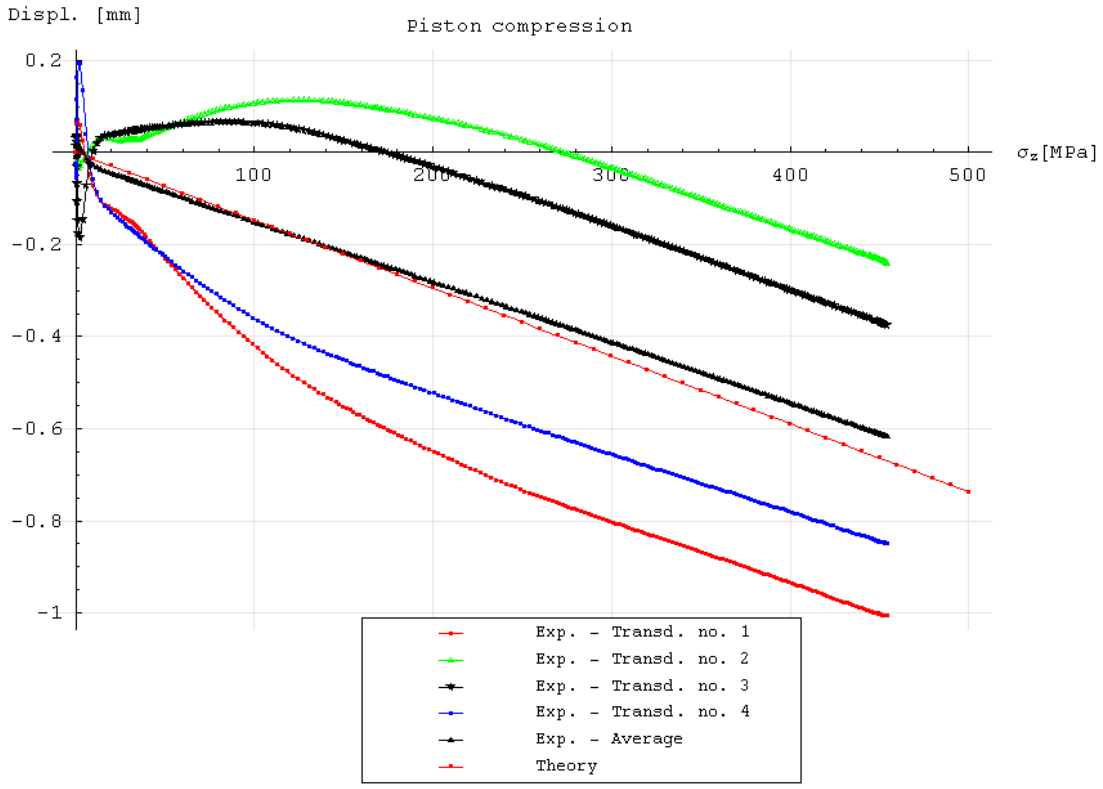

Figure 7.1: The measured compression of the piston and the theoretical values.

As can be seen the apparatus is bending when compressing the upper and lower piston together. Taking the average of the output from the four displacement transducers we get a fairly good match with the theoretical calculation. The discrepancy between the experimental average and theory is probably due to some nonlinear behavior of the transducers.

8 Friction along the inner cylindrical wall

What can be done when friction applies between the unknown material and the steel cylinder along the walls of the cylinder and where compaction of the unknown material is large and leading to complicated boundary conditions?

The question is whether the friction and expansion of the cylinder invalidate equation (4.1). In section 5 we showed that the bulging of the cylinder due to test sample only being in contact with the cylinder in a small region (see figure 2.1) did not invalidate the equation (4.1) significantly. But the friction could in principle do this. The friction decreases the axial stress in the test sample along the distance from the upper moving piston. Thus the radial stress also decreases with the distance from the upper loading piston. For most situations we assume that the formula (4.20) still can be used.

Without radial expansion, the axial stress in the cylinder should be caused by the shear forces caused by the friction along the inner walls. We have in the theoretical analyses used that the axial stress is independent of the radial coordinate *r*.

The shear force must be equal to the difference between the force on the bottom and top piston, to read

$$S = A_w \tau_z = F^{bot} - F^{top} \Rightarrow \tau_z = -\frac{F^{top} - F^{bot}}{A_w}, \quad A_w = 2\pi R_1 h \tag{8.1}$$

But the shear stress is not constant along the inner surface of the steel cylinder so formula (8.1) has only limited value. The shear stress is actually decreasing with the depth from the sample surface. Figure 8.1 shows the calculated shear force by using equation (8.1). In equation (8.1) *h* is the height of the test sample which vary with the load.

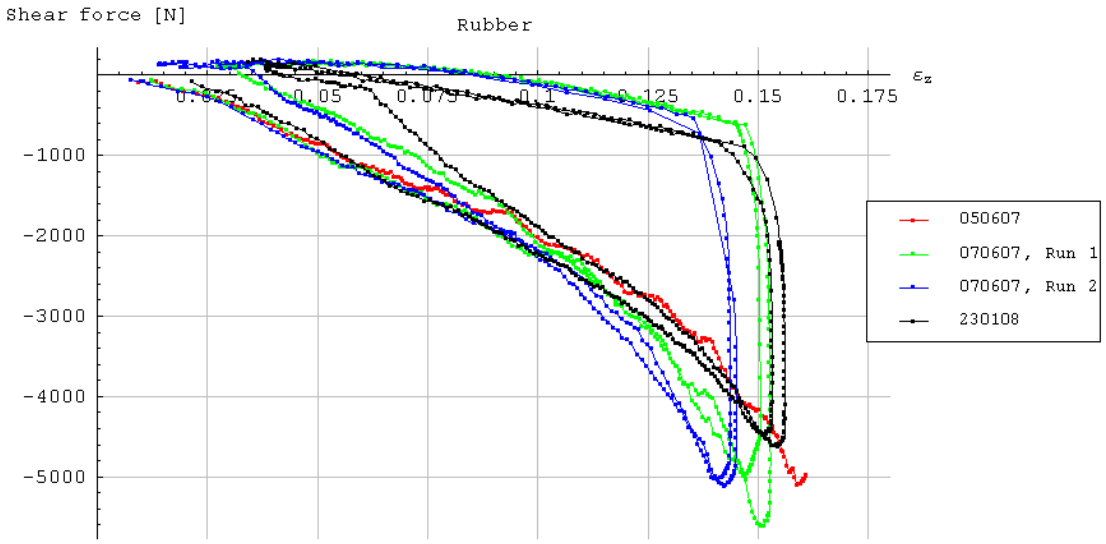

Figure 8.1: Measured shear force as a function of axial strain of the sample.

Assume that the axial stress is significantly lower at the bottom of the sample du to friction along the walls. We forecast the following equation as a model for the average axial stress in the test sample

$$\underbrace{\sigma_z}_{\substack{\text{assumed axial} \\ \text{stress in sample}}} \overset{mod}{=} \frac{1}{2}\left(\underbrace{F^{top}/A_0}_{top} + \underbrace{F^{bot}/A_0}_{bottom} \right), \tag{8.2}$$

To achieve this quantity we measure the force at the top and bottom of the material. To seek out the average radial stress experimentally we assume that we must place the strain gauges close to the middle of the compressed material.

The coefficient of friction can be calculated. According to the Janssen approach we could use the following equation for the stresses in the sample as a function of the axial displacement

$$\begin{aligned} &\pi R_1^2\left(\sigma_z(z+dz)-\sigma_z(z)\right) \overset{mod}{=} -2\pi R_1 \tau_z dz = -2\pi R_1 \mu \sigma_r dz = -2\pi R_1 \mu k \sigma_z dz \\ &\Rightarrow \frac{\partial \sigma_z}{\partial z} = -\frac{2\mu k}{R_1}\sigma_z,\ \tau_z \overset{mod}{=} \mu\sigma_r,\ k \overset{def}{=} \frac{\sigma_r}{\sigma_z} \end{aligned} \tag{8.3}$$

μ is the coefficient of friction. We have applied the traditional laws of friction where the friction force is proportional to the normal force.

We further assume as a first approximation that $\partial k/\partial z \overset{mod}{=} 0$. The reason for this assumption is that during compression without friction the *k* fraction is not varying significantly with the load. This follows from figure 5.4 which show a small variation of *k/(1+k)* with the load. When

friction applies along the inner cylindrical wall, the axial stress is decreasing with the depth from the upper surface of the test sample. Equation (8.3) gives the solution

$$\sigma_z = \sigma_z^{top} Exp\left(-\frac{2\mu k}{R_1} z\right) \tag{8.4}$$

This gives that the stress at the bottom of the test sample becomes

$$\sigma_z(z=h) = \sigma_z^{bot} = \sigma_z^{top} Exp\left(-\frac{2\mu k}{R_1} h\right) \tag{8.5}$$

where h is the height of the test sample. The coefficient of friction then becomes equal to

$$\mu = \frac{R_1}{2k(t)\,h(t)} Ln\left(\frac{\sigma_z^{top}(t)}{\sigma_z^{bot}(t)}\right),\ k = \frac{\sigma_r(t)}{\sigma_z(t)} \tag{8.6}$$

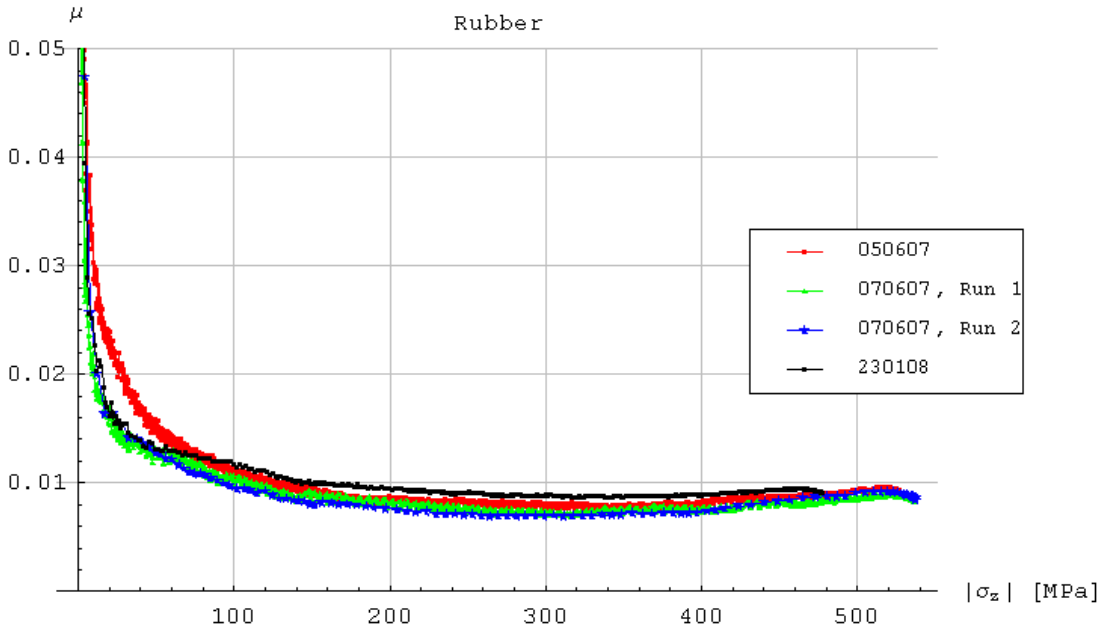

Figure 8.2: The coefficient of friction, μ, as a function of the axial stress in the sample (rubber). The three first samples in this figure were covered with a thin tissue paper to minimize the friction.(7.6)

Figure 8.2 shows the measured coefficient of friction. It is quite low and decreasing until about an axial stress of 340 MPa and then it increases slightly.

The radial stress is only available at the middle of the sample due to the position of the gauges. The axial stress at the middle of the sample now becomes

$$\sigma_z(z=h/2)=\sigma_z^{top}Exp\left(-\frac{\mu k}{R_1}h\right)\approx\sigma_z^{top}\left(1-\frac{\mu k}{R_1}h\right)$$

$$\frac{1}{2}\left(\sigma_z^{top}+\sigma_z^{bot}\right)=\frac{1}{2}\left(\sigma_z^{top}+\sigma_z^{top}Exp\left(-\frac{2\mu k}{R_1}h\right)\right)=\frac{1}{2}\sigma_z^{top}\left(1+Exp\left(-\frac{2\mu k}{R_1}h\right)\right) \tag{8.7}$$

$$\approx\sigma_z^{top}\left(1-\frac{\mu k}{R_1}h\right)\approx\sigma_z(z=h/2)$$

Thus the axial stress at the middle approximately becomes the average stress of the top and bottom, in agreement with equation (8.2). Thus the *k* factor is then given approximately by the equation

$$k=\frac{\sigma_r(t)}{\sigma_z(t)}=\frac{2\sigma_r(t)}{\left(\sigma_z^{top}(t)+\sigma_z^{bot}(t)\right)} \tag{8.8}$$

The radial stress is calculated by the equation (4.21). The *k* factor is inserted into equation (8.6) to give the friction coefficient.

9 Cyclic variation

In this section we outline the model that is used to simulate cyclic variation in the load on the test sample.

We let the displacement of the transducer be given externally. Thus strain and density become a function of time equal to

$$\rho(t)=\rho_0\ h_0/h(t),\ \ \varepsilon_z(t)=-Ln\left(\frac{\rho(t)}{\rho_0}\right)=-Ln\left(\frac{h_0}{h(t)}\right) \tag{9.1}$$

The change in the strain becomes

$$\Delta\varepsilon_z(t)=\varepsilon_z\left(t+\Delta t\right)-\varepsilon_z\left(t\right) \tag{9.2}$$

The reduced strains and the effective strain are then calculated by

$$
\begin{aligned}
&e_z(t) = \frac{2}{3}\varepsilon_z\left(t\right), \Delta e_z(t) = e_z\left(t+\Delta t\right) - e_z\left(t\right), \\
&e_r(t) = -\frac{1}{3}\varepsilon_z\left(t\right), \Delta e_r(t) = e_r\left(t+\Delta t\right) - e_r\left(t\right), \\
&e_\theta(t) = -\frac{1}{3}\varepsilon_z\left(t\right), \Delta e_\theta(t) = e_\theta\left(t+\Delta t\right) - e_\theta\left(t\right) \\
&e_{eff}(t) = \left(\frac{2}{3}\left(e_r(t)^2 + e_\theta(t)^2 + e_z(t)^2\right)\right)^{1/2} = Abs\left(e_z(t)\right)
\end{aligned}
\tag{9.3}
$$

The forecast pressure becomes

$$
p^f(t+\Delta t) \overset{mod}{=} p(t) - K\left(\rho(t)\right)\Delta\varepsilon_z(t) : \text{forecast} \tag{9.4}
$$

where K is the elastic bulk modulus assumed to be a function of the density.

The compaction curve is assumed to be given by

$$
P_c\left(\rho\right) \overset{mod}{=} K\left(\rho/\rho_0 - 1\right) = K\left(Exp\left(-\varepsilon_z\right) - 1\right) \approx -K\varepsilon_z : \text{Generally} \tag{9.5}
$$

The new pressure is calculated by the algorithm

$$
\begin{aligned}
&\text{If } p^f(t+\Delta t) \text{ larger or equal } P_c\left(\rho(t+\Delta t)\right) \\
&p(t+\Delta t) = P_c\left(\rho(t+\Delta t)\right) \\
&\text{else} \\
&p(t+\Delta t) = p^f(t+\Delta t) \\
&\text{end}
\end{aligned}
\tag{9.6}
$$

The volumetric plastic increment $\varepsilon_z^{vp}(t)$ is given by

$$
\begin{aligned}
&\Delta\varepsilon^{vp}(t) = \Delta\varepsilon_z^{vp}(t) = \Delta\varepsilon_z(t) + \Delta p(t)/K,\ \Delta p(t) \overset{def}{=} p(t+\Delta t) - p(t) \\
&\varepsilon_z^{vp}(t+\Delta t) \overset{mod}{=} \varepsilon_z^{vp}(t) + \Delta\varepsilon_z^{vp}(t)
\end{aligned}
\tag{9.7}
$$

The forecast deviatoric stress is given by

$$
\begin{aligned}
&s_z{}^f(t+\Delta t) = s_z(t) + 2G\left(\rho(t)\right)\Delta e_z(t) : \text{forecast} \\
&s_r{}^f(t+\Delta t) = s_\theta{}^f(t+\Delta t) = -\frac{1}{2}s_z{}^f(t+\Delta t)
\end{aligned}
\tag{9.8}
$$

where G is the elastic bulk modulus assumed to be a function of the density. The forecast effective stress (von Mises) is given by the algorithm

$$\sigma_{eff}^{f}\left(t+\Delta t\right)=\left(\frac{3}{2}\right)^{1/2}\left\|\overline{s}^{f}\left(t+\Delta t\right)\right\|=\frac{3}{2}Abs\left({s_z}^{f}\left(t+\Delta t\right)\right),$$
$$\left\|\overline{s}^{f}\left(t+\Delta t\right)\right\|\overset{def}{=}\left({s_z}^{f}\left(t+\Delta t\right)^2+{s_r}^{f}\left(t+\Delta t\right)^2+{s_\theta}^{f}\left(t+\Delta t\right)^2\right)^{1/2} \tag{9.9}$$

The flow stress is given by the functionality

$$Y\left(p(t),e_{eff}^{p}(t)\right) \tag{9.10}$$

The deviatoric stresses are calculated by

If $\sigma_{eff}^{f}\left(t+\Delta t\right)$ larger or equal $Y\left(p(t),e_{eff}^{p}(t)\right)$

$$s_z(t+\Delta t)=\left(\frac{2}{3}\right)^{1/2}\frac{s_z^{f}(t+\Delta t)}{\left\|\overline{s}^{f}\left(t+\Delta t\right)\right\|}Y\left(p(t),e_{eff}^{p}(t)\right)$$
$$s_r(t+\Delta t)=\left(\frac{2}{3}\right)^{1/2}\frac{s_r^{f}(t+\Delta t)}{\left\|\overline{s}^{f}\left(t+\Delta t\right)\right\|}Y\left(p(t),e_{eff}^{p}(t)\right)$$
$$s_\theta(t+\Delta t)=\left(\frac{2}{3}\right)^{1/2}\frac{s_\theta^{f}(t+\Delta t)}{\left\|\overline{s}^{f}\left(t+\Delta t\right)\right\|}Y\left(p(t),e_{eff}^{p}(t)\right) \tag{9.11}$$

else

$$s_z(t+\Delta t)={s_z}^{f}(t+\Delta t), s_r(t+\Delta t)={s_r}^{f}(t+\Delta t), s_\theta(t+\Delta t)={s_\theta}^{f}(t+\Delta t)$$

end

Notice that during unilateral compression $\left\|\overline{s}^{f}\left(t+\Delta t\right)\right\|=\left(3/2\right)^{1/2}Abs\left({s_z}^{f}\left(t+\Delta t\right)\right)$, according to equation (9.9). Thus we can write (9.11) as

If $\sigma_{eff}^{f}\left(t+\Delta t\right)$ larger or equal $Y\left(p(t),e_{eff}^{p}(t)\right)$

$$s_z(t+\Delta t)=\frac{2}{3}Sign\left(s_z^{f}(t+\Delta t)\right)Y\left(p(t),e_{eff}^{p}(t)\right)$$

else

$$s_z(t+\Delta t)={s_z}^{f}(t+\Delta t) \tag{9.12}$$

end

$$s_r(t+\Delta t)=s_\theta(t+\Delta t)=-\frac{1}{2}s_z(t+\Delta t)$$

The deviatoric plastic strains are calculated by

$$
\begin{aligned}
&\Delta e_z^p(t) = \Delta e_z(t) - \Delta s_z(t)/2G,\ \Delta s_z(t) = s_z(t+\Delta t) - s_z(t)\\
&\Delta e_r^p(t) = \Delta e_r(t) - \Delta s_r(t)/2G = -\frac{1}{2}\Delta e_z^p(t),\\
&\Delta e_\theta^p(t) = \Delta e_\theta(t) - \Delta s_\theta(t)/2G = -\frac{1}{2}\Delta e_z^p(t),\\
&e_z^p(t+\Delta t) = e_z^p(t) + \Delta e_z^p(t)\\
&e_r^p(t+\Delta t) = e_z^p(t) + \Delta e_z^p(t) = -\frac{1}{2}e_z^p(t+\Delta t)\\
&e_\theta^p(t+\Delta t) = -\frac{1}{2}e_z^p(t+\Delta t)
\end{aligned}
\tag{9.13}
$$

The effective plastic strain becomes

$$
e_{eff}^p(t+\Delta t) = \left(\frac{2}{3}\left(e_r^p(t+\Delta t)^2 + e_\theta^p(t+\Delta t)^2 + e_z^p(t+\Delta t)^2\right)\right)^{1/2} = Abs\left(e_z^p(t+\Delta t)\right) \tag{9.14}
$$

Note that the model in this section is of the non-associative type.

We could write equation (9.11) generally as

$$
\begin{aligned}
&s_{ij}^f\left(t+\Delta t\right) = s_{ij}\left(t\right) + 2G\Delta e_{ij}(t)\\
&\sigma_{eff}^f\left(t+\Delta t\right) = \left(\frac{3}{2}\right)^{1/2}\left\|\overline{s}^f(t+\Delta t)\right\|, \left\|\overline{s}^f(t+\Delta t)\right\| \overset{def}{=} \left(s_{ij}{}^f(t+\Delta t)s_{ij}{}^f(t+\Delta t)\right)^{1/2}\\
&If\ \sigma_{eff}^f\left(t+\Delta t\right) \text{ larger or equal } Y\left(p(t), e_{eff}^p(t)\right)\\
&s_{ij}(t+\Delta t) = \left(\frac{2}{3}\right)^{1/2}\frac{s_{ij}^f(t+\Delta t)}{\left\|\overline{s}^f(t+\Delta t)\right\|}Y\left(p(t), e_{eff}^p(t)\right)
\end{aligned}
\tag{9.15}
$$

else

$$
s_{ij}(t+\Delta t) = s_{ij}{}^f(t+\Delta t)
$$

end

An alternative formulation that is not exactly the same is

If $\sigma_{eff}^{f}\left(t+\Delta t\right)$ larger or equal $Y\left(p(t),e_{eff}^{p}(t)\right)$

$$s_{ij}(t+\Delta t)=\left(\frac{2}{3}\right)^{1/2} Y\,\Delta e_{ij}(t)/\left\|\Delta\overline{e}(t)\right\|$$

else (9.16)

$$s_{ij}(t+\Delta t)=s_{ij}{}^{f}(t+\Delta t)=s_{ij}\ (t)+2G\Delta e_{ij}(t)=2G\left(e_{ij}(t+\Delta t)-e_{ij}(t)\right)$$

end

We could write that $\Delta e_{ij}(t)/\left\|\Delta\overline{e}(t)\right\|=\left(a_{ij}(t)+2G\Delta e_{ij}(t)\right)/\left\|a_{ij}(t)+2G\Delta e_{ij}(t)\right\|$ when $a_{ij}(t)\propto\Delta e_{ij}(t)$. To reach correspondence with equation (9.15) we must have that during plastic flow $s_{ij}(t)\propto\Delta e_{ij}(t)$. This is not quite correct since only $s_{ij}(t+\Delta t)\propto\Delta e_{ij}(t)$. The discrepancy of the two models does not show up in simple compression/tension or unilateral compression/tension.

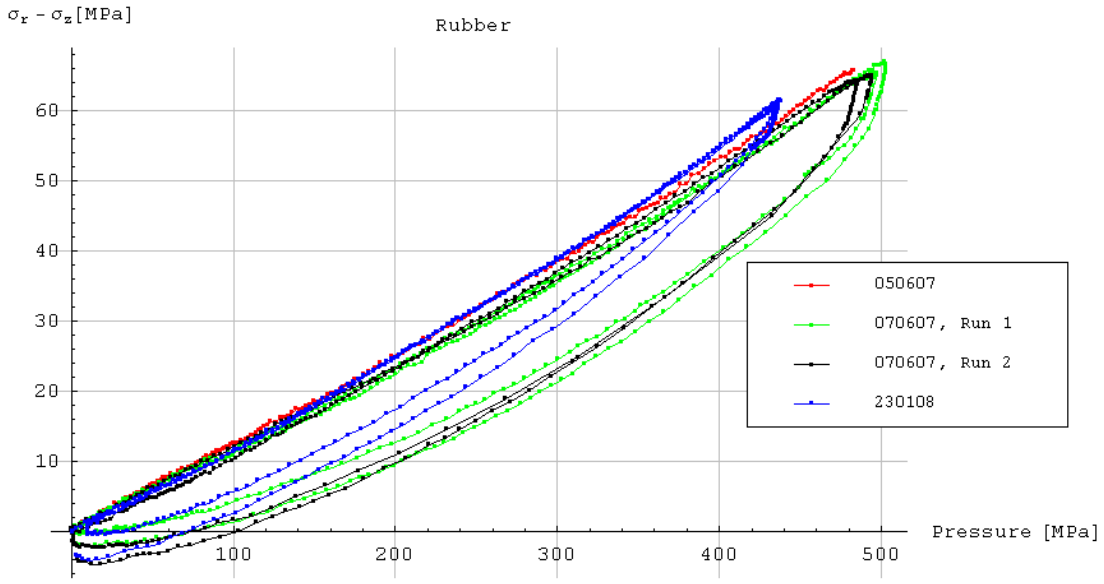

Figure 9.1: Mises stress of rubber as a function of pressure during cyclic loading.

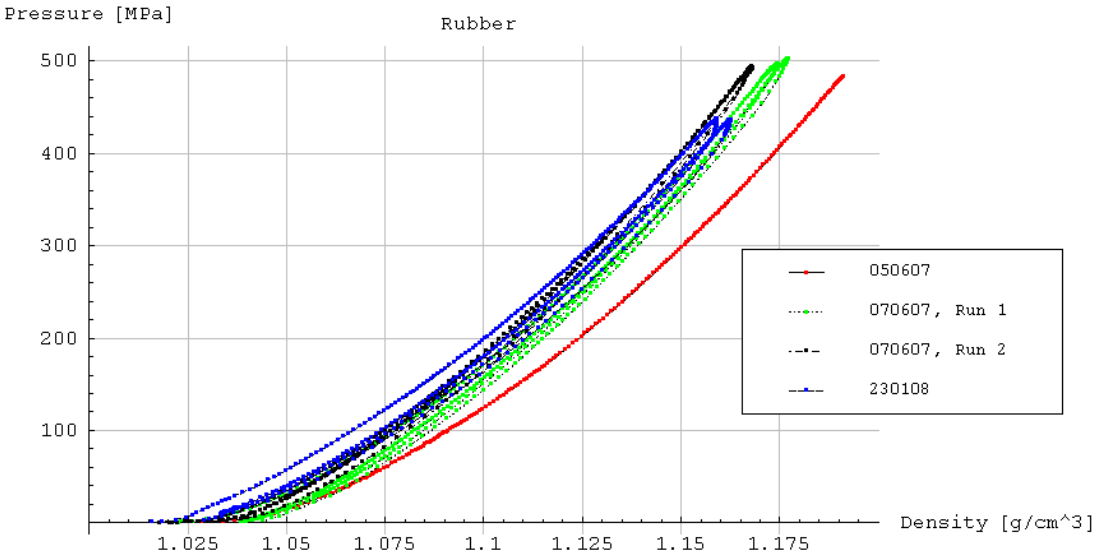

Figure 9.2: Pressure as a function of density during cycling loading.

10 A cap model

In this section we outline (suggest) a cap model. The "forecast stress " is given by

$$\begin{aligned}
\sigma_z^f(t+\Delta t) &= p(t) - K\big(\rho(t)\big)\Delta\varepsilon_z(t) + s_z(t) + 2G\big(\rho(t)\big)\Delta e_z(t) \\
\sigma_r^f(t+\Delta t) &= p(t) - K\big(\rho(t)\big)\Delta\varepsilon_z(t) + s_r(t) - G\big(\rho(t)\big)\Delta e_z(t) \\
s_r{}^f(t+\Delta t) &= s_\theta{}^f(t+\Delta t) = -\frac{1}{2}s_z{}^f(t+\Delta t)
\end{aligned} \tag{10.1}$$

The scaling during volumetric and deviatoric plastic flow is given by

$$
\begin{aligned}
&\textit{If } \psi_{eff}^{f}\left(t+\Delta t\right) \textit{ larger or equal } \Pi\left(\rho(t+\Delta t), p(t+\Delta t), e_{eff}^{p}(t)\right)\\
&\sigma_z(t+\Delta t)=\frac{\sigma_z^{f}(t+\Delta t)}{\|\bar{\sigma}\|}\Pi\left(\rho(t+\Delta t), p(t+\Delta t), e_{eff}^{p}(t)\right)\\
&\sigma_r(t+\Delta t)=\frac{\sigma_r^{f}(t+\Delta t)}{\|\bar{\sigma}\|}\Pi\left(\rho(t+\Delta t), p(t+\Delta t), e_{eff}^{p}(t)\right)\\
&\sigma_r(t+\Delta t)=\sigma_\theta(t+\Delta t)\\
&\textit{else}\\
&\sigma_z(t+\Delta t)=\sigma_z{}^{f}(t+\Delta t), \sigma_r(t+\Delta t)=\sigma_r{}^{f}(t+\Delta t), \sigma_\theta(t+\Delta t)=\sigma_\theta{}^{f}(t+\Delta t)\\
&\textit{end}\\
&\psi_{eff}^{f}\left(t+\Delta t\right)=\|\bar{\sigma}\|=\left(\sigma_z{}^{f}(t+\Delta t)^2+2\sigma_r{}^{f}(t+\Delta t)^2\right)^{1/2},
\end{aligned}
\tag{10.2}
$$

Notice that we plot $\left(\sigma_z{}^{f}(t+\Delta t)^2+2\sigma_r{}^{f}(t+\Delta t)^2\right)^{1/2}$ to find the flow function.

During unloading the elastic part is found.

11 Models for glass spheres

In this section we outline the material properties for a powder of glass spheres.

Figure 11.1 show the glass spheres before the GREAC cell test. In figure 11.2 the test has been carried out. It is seen that some glass spheres has been crushed and some is still intact. The spheres have a size of approximately 40 to 85 μm.

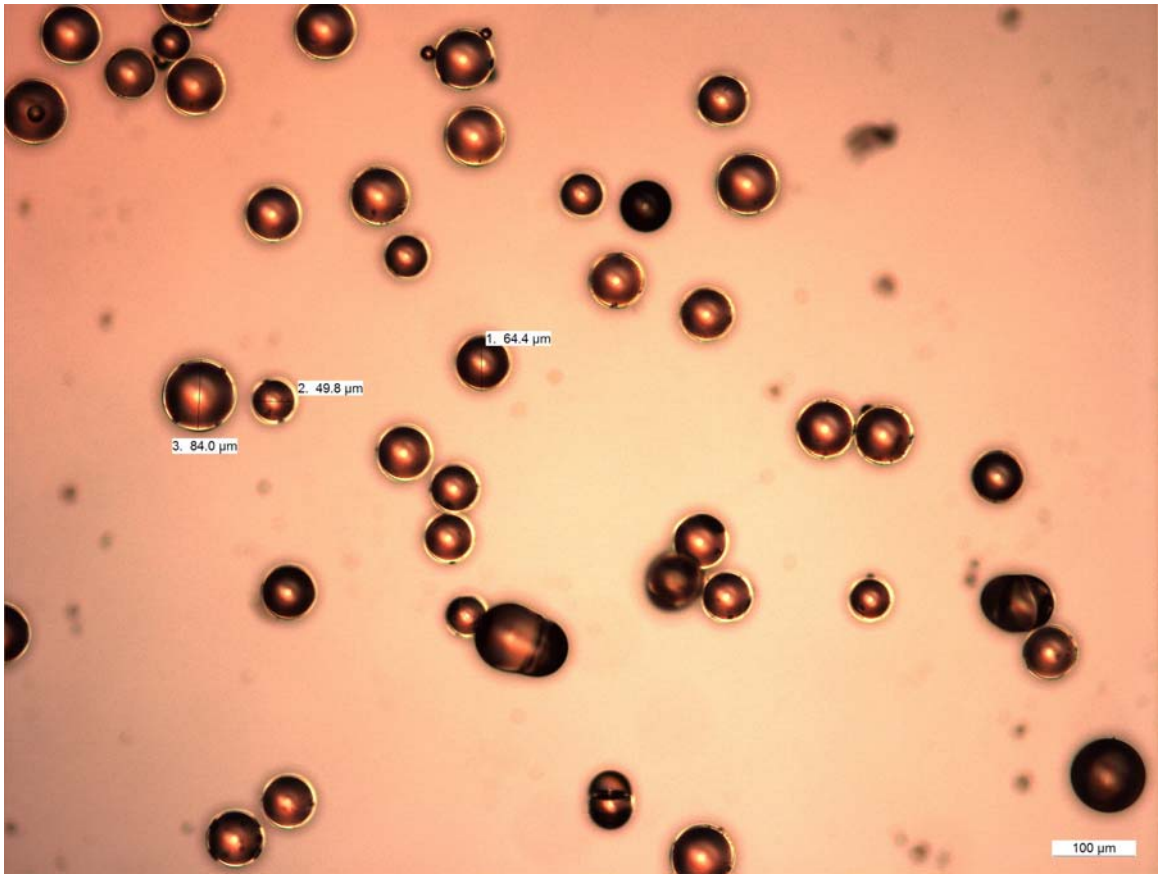

Figure 11.1: Glass spheres before loading.

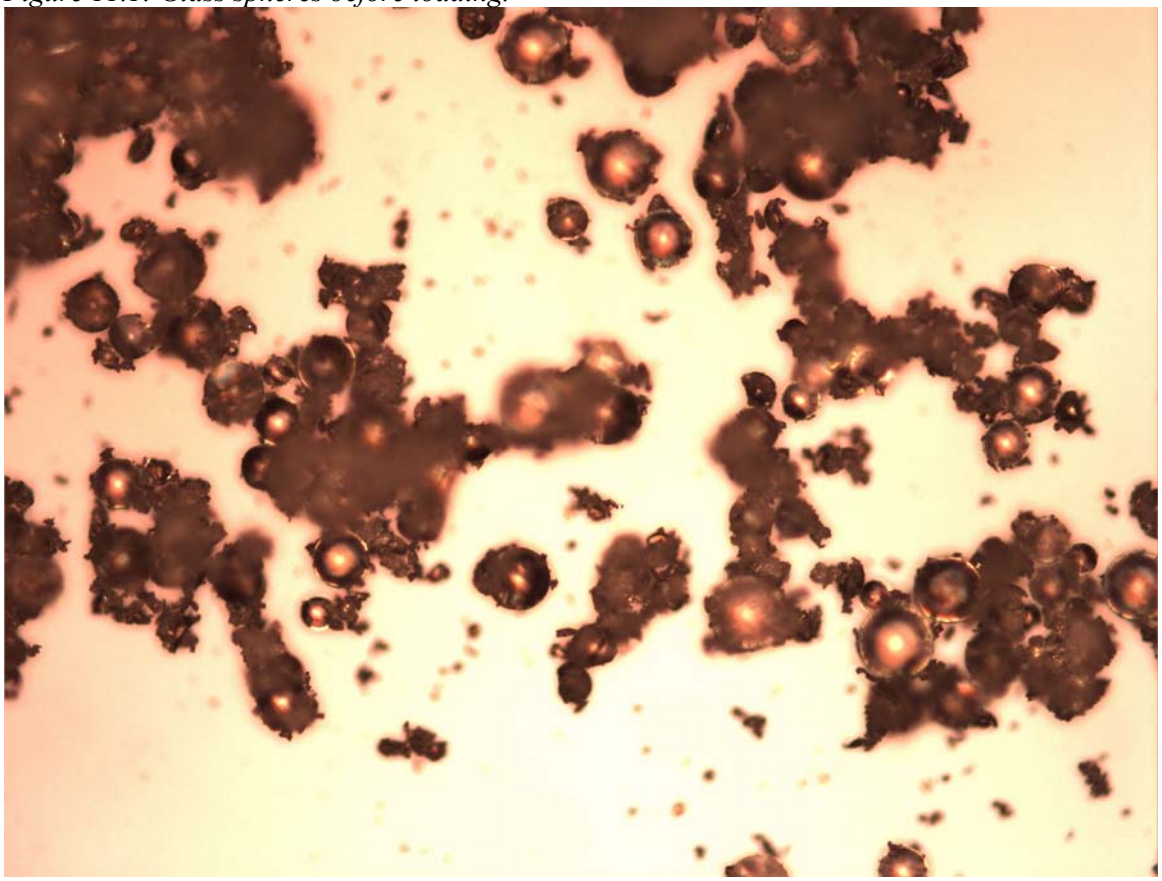

Figure 11.2: Glass spheres after loading.

11.1 Experimental results

The difference between applied and transmitted stress for the glass spheres during loading in the GREAC cell is shown in figure 11.3. The glass powder shows friction against the cylindrical walls. Some glass powder is observed to move into the gap between the moving upper piston and the confining cylinder thus probably creating a part of this friction. The average value of the applied and transmitted load has been used in the calculations for the von Mises stress, pressure etc.

Figure 11.3: Applied and transmitted stress.

We observe that there is hysteresis during loading and unloading (figures 11.4). Figure 11.4 shows the Mises stress as a function of the density for different experimental runs. The Mises stress as a function of the pressure is shown in figure 11.5. We will come back to an interpretation of this when we compare the numerical model with the experimental results.

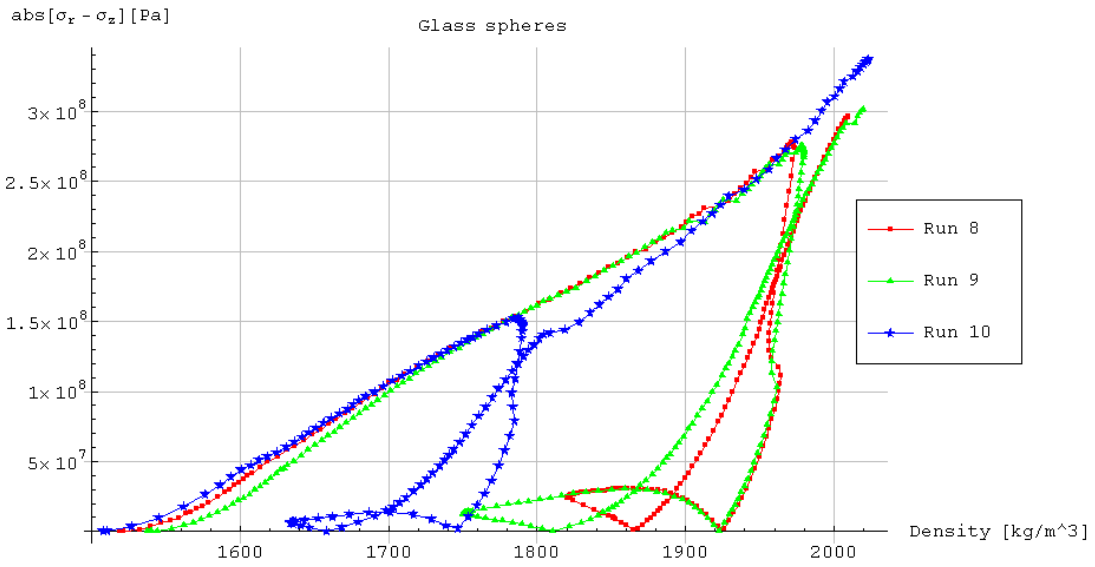

Figure 11.4: The Mises stress as a function of the density.

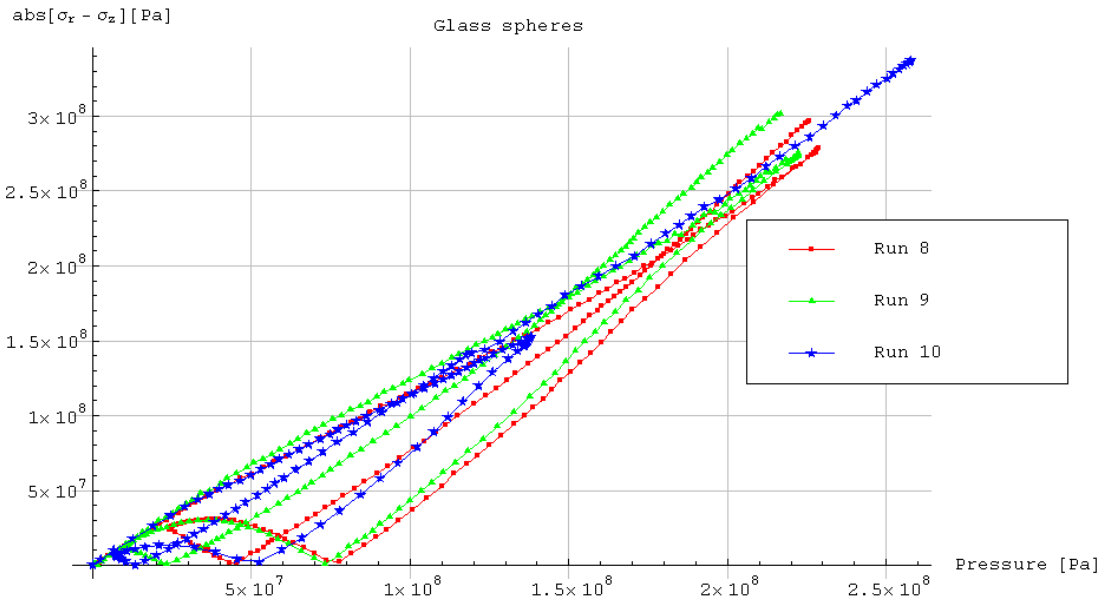

Figure 11.5: The Mises stress as a function of the pressure.

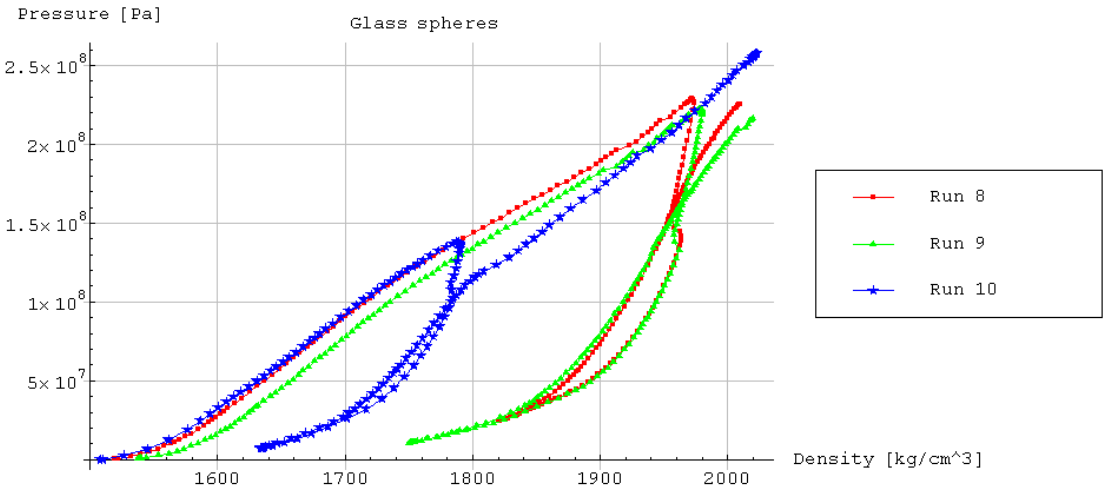

Figure 11.6: The pressure as a function of the density.

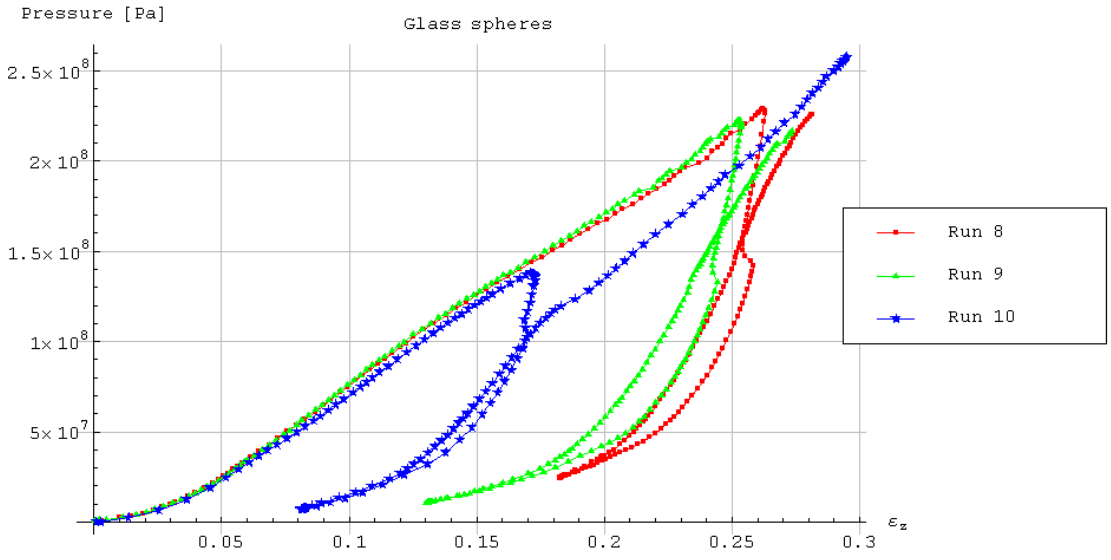

Figure 11.7: The pressure as a function of the axial strain.

11.2 Numerical results

When constructing the model we compare theoretical results with experimental results. The objective is to get a good fit. But the theoretical results are mainly constructed on the unilateral compression assumption, i.e. no friction along the walls of the cylinder and small outward bulging of the cylinder. Actually, a complete theoretical model needs simulations of the whole loading apparatus with friction. We have performed this and some results are reported in section 12.

The model for glass spheres is specified by 4 input functions.
1) The shear modulus as a function of density (figure 11.8).
2) The bulk modulus as a function of density (figure 11.9).
The Poisson's ratio then follows as shown in subtitle to figure 11.10. We study the Poisson's ratio to be certain that the shear modulus and the bulk modulus are trustworthy (chapter 4).

3) The yield stress as a function of density and as a function of pressure.
We have chosen a pressure dependency only (figure 11.11). During unloading from high stresses the material initially becomes elastic, but finally become plastic. The unloading curve is also shown in figure 11.11. When loading again the material is elastic initially but become plastic after large stresses. Notice the hysteresis in figure 11.11. Also notice that the material does not reach a state of no stress during unloading.

4) The compaction curve, i.e. the pressure as a function of the density (figure 11.12).
This curve is shown in figure 11.12. Figure 11.12 also show an unloading path. Notice that the pressure does not reach a state of no pressure.

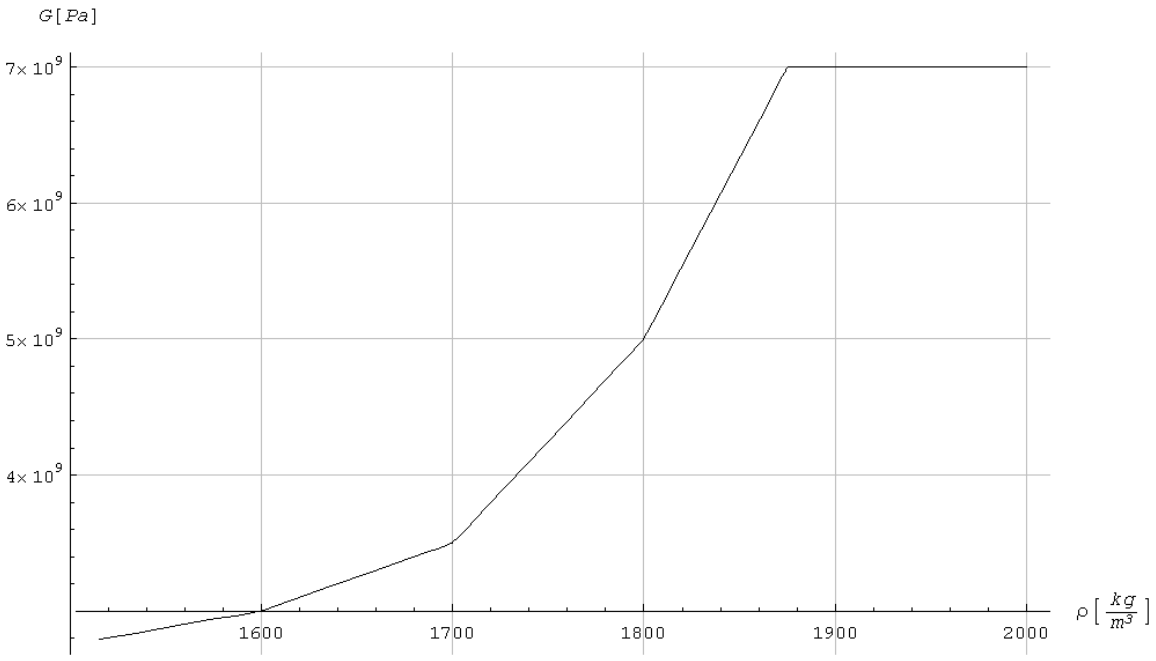

Figure 11.8: G(ρ)= {{1515, 2.79 10^9}, {1600, 3 10^9}, {1700, 3.5 10^9}, {1800, 5 10^9}, {1875, 7 10^9}, {2000, 7 10^9}}, shear modulus as a function of density.

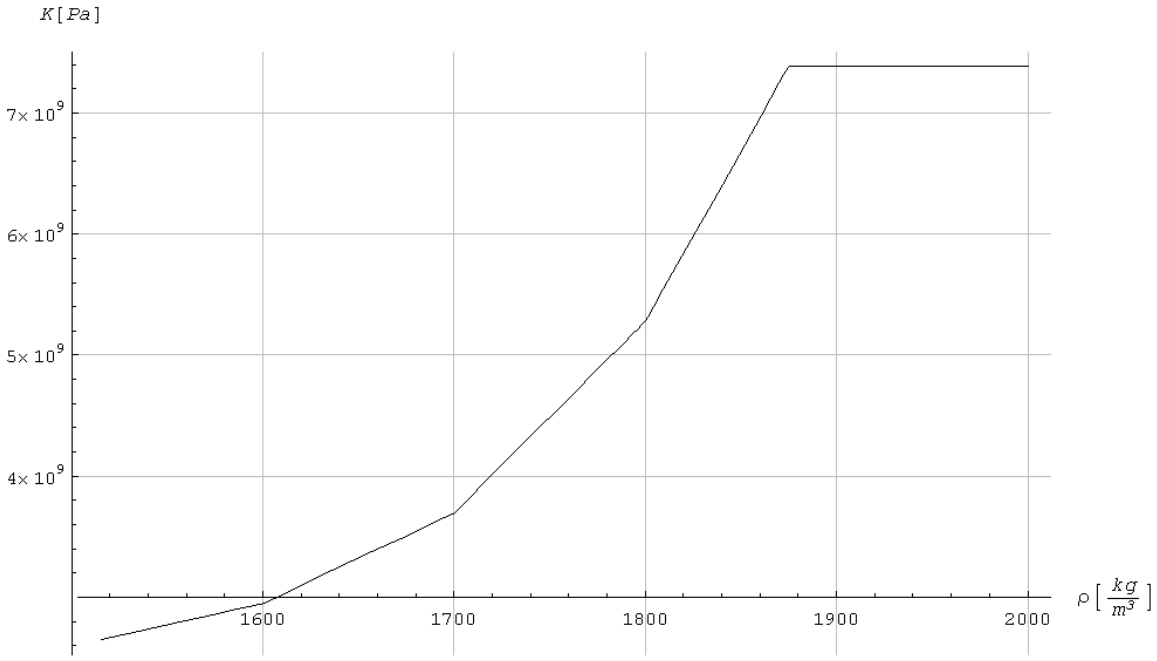

Figure 11.9: K(ρ)= {{1515, 2.65 10^9}, {1600, 2.95 10^9}, {1700, 3.69 10^9}, {1800, 5.28 10^9}, {1875, 7.39 10^9}, {2000, 7.39 10^9}}, bulk modulus as a function of density.

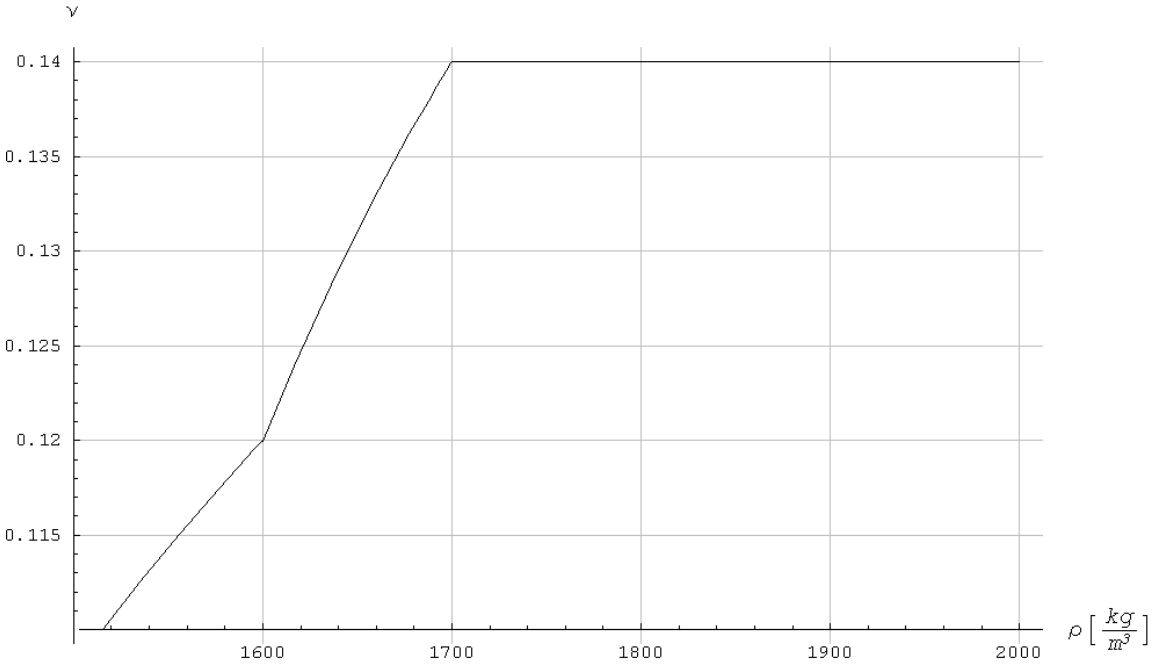

Figure 11.10: ν(ρ)=(3 K(ρ) - 2 G(ρ))/(6 K(ρ) + 2 G(ρ)), Poisson's ratio as a function of density.

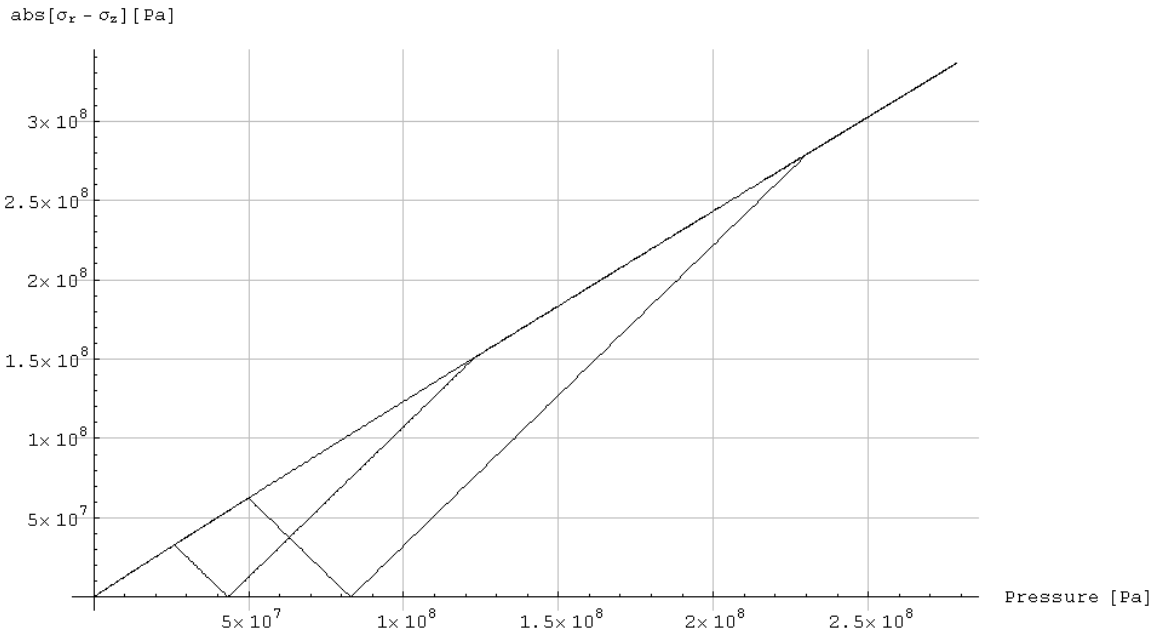

Figure 11.11: Mis(p)= 1.25 · 5 10^7/ (5 10^7)$^{0.98}$ $p^{0.98}$, yield stress as a function of pressure.

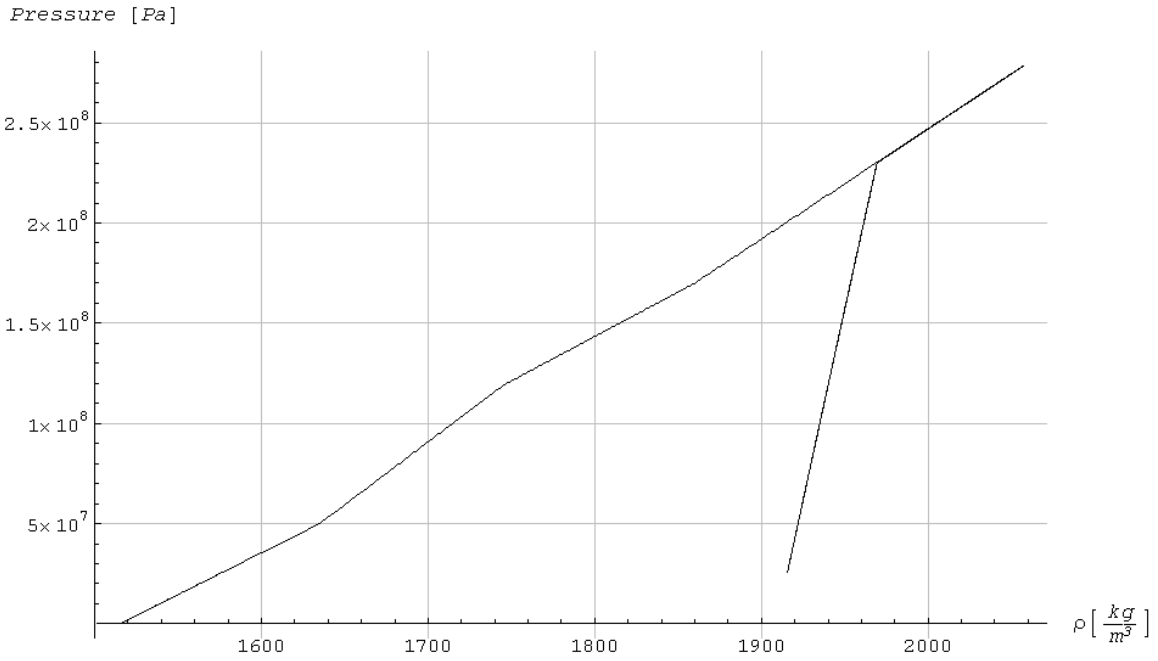

Figure 11.12: p(ρ)= { {1515, 10^5},{1635,5 10^7},{1745, 1.19 10^8},{1860, 1.7 10^8},{1960, 2.25 10^8}}, pressure as a function of density (the compaction curve).

11.3 Experimental vs. numerical results

Run 8

Specific properties for this run were as following. Mass of sample was 0.005744 kg and initial height of sample was 0.0167 m. The maximum displacement used in the numerical analysis before unloading was -0.00385 m, and the displacement at reloading was -0.00349 m.

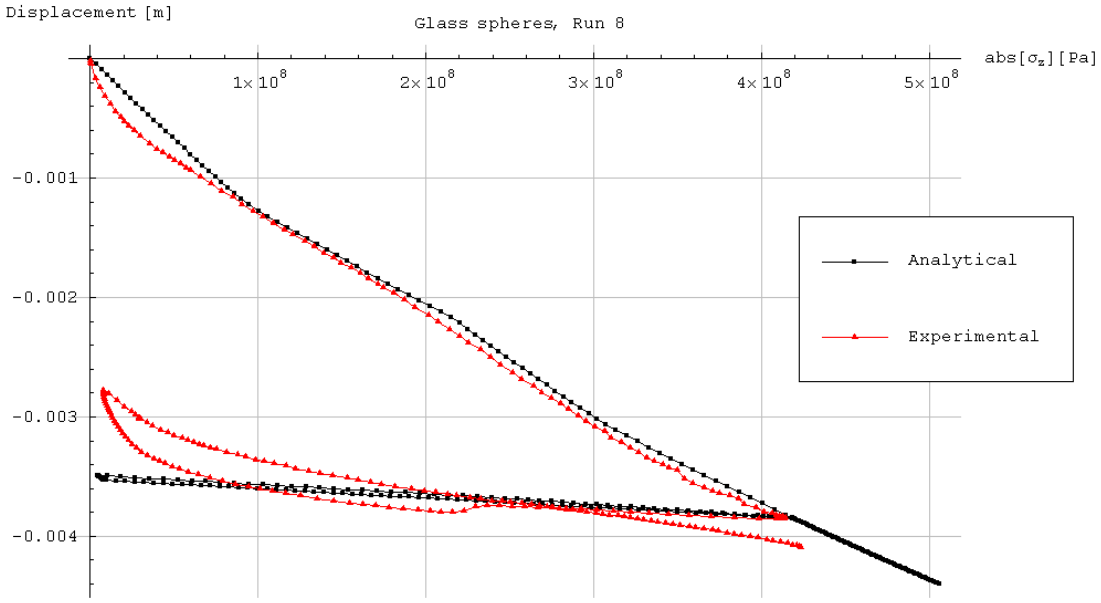

Figure 11.13: Displacement used in numerical analysis vs. experimental measurements.

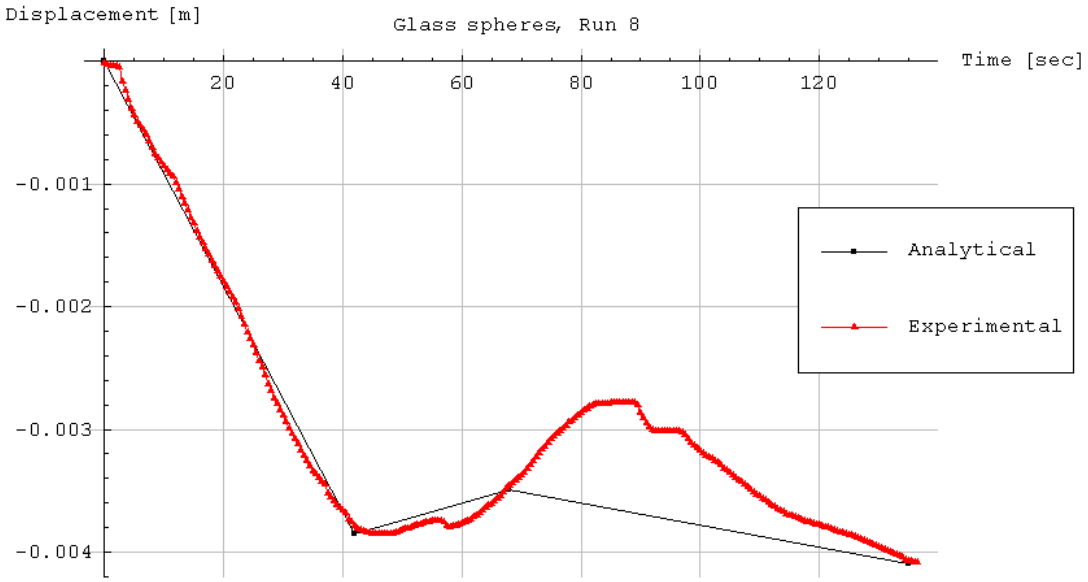

Figure 11.14: Displacement as a function of time.

Figure 11.15 shows simulation results for the pressure, axial stress and the radial stress as a function of the axial strain in the sample. Notice the hysteresis during unloading/loading.

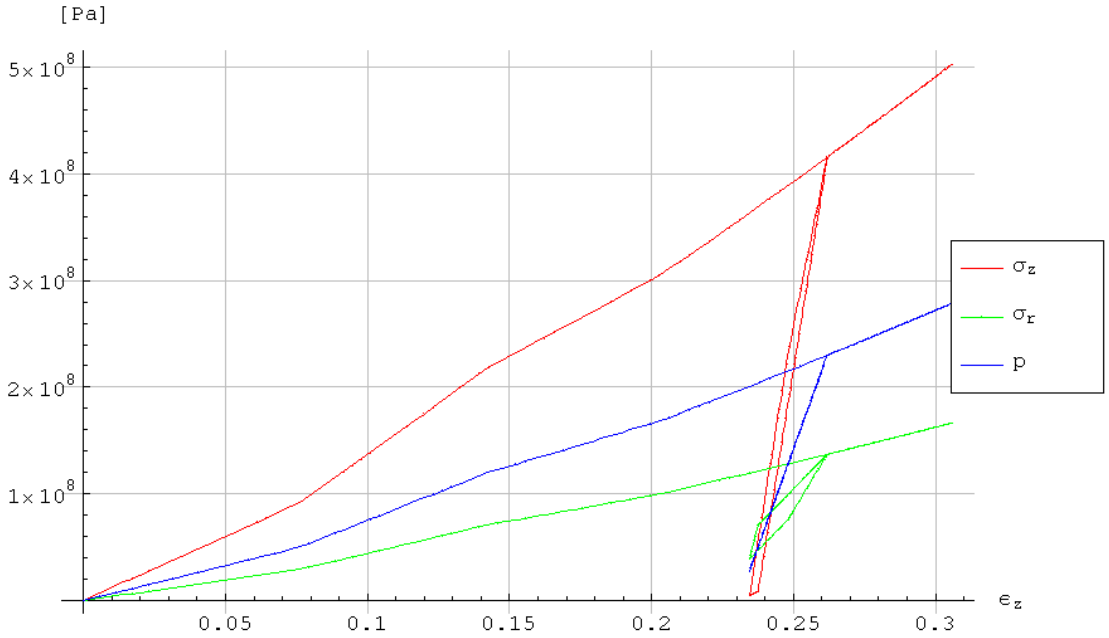

Figure 11.15: Numerical results of pressure, axial stress and the radial stress as a function of the axial strain in the sample.

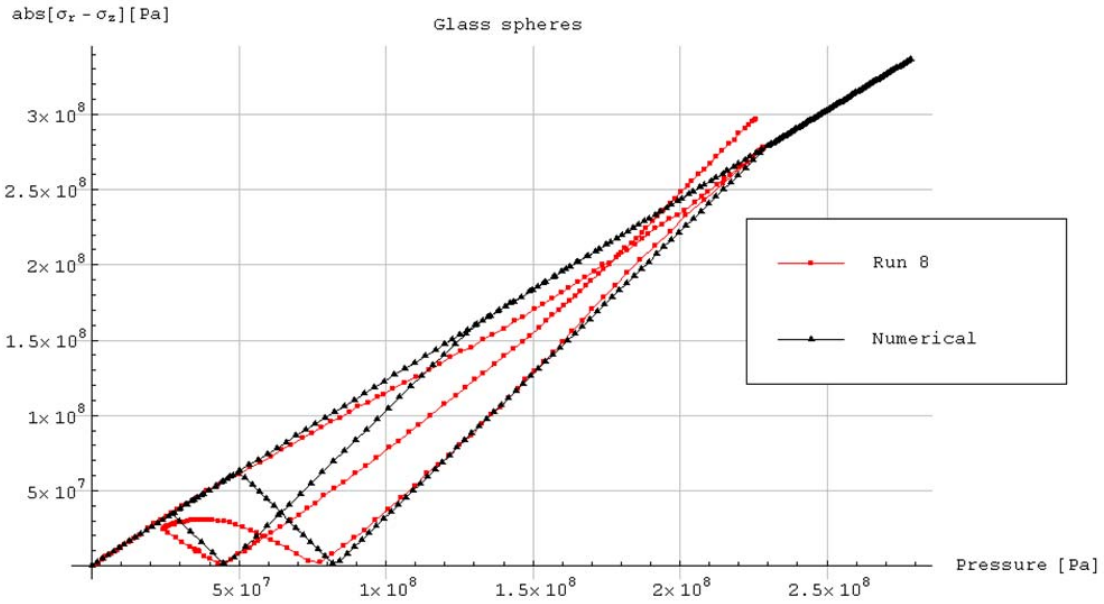

Figure 11.16: Mises stress as a function of pressure for experimental and numerical results.

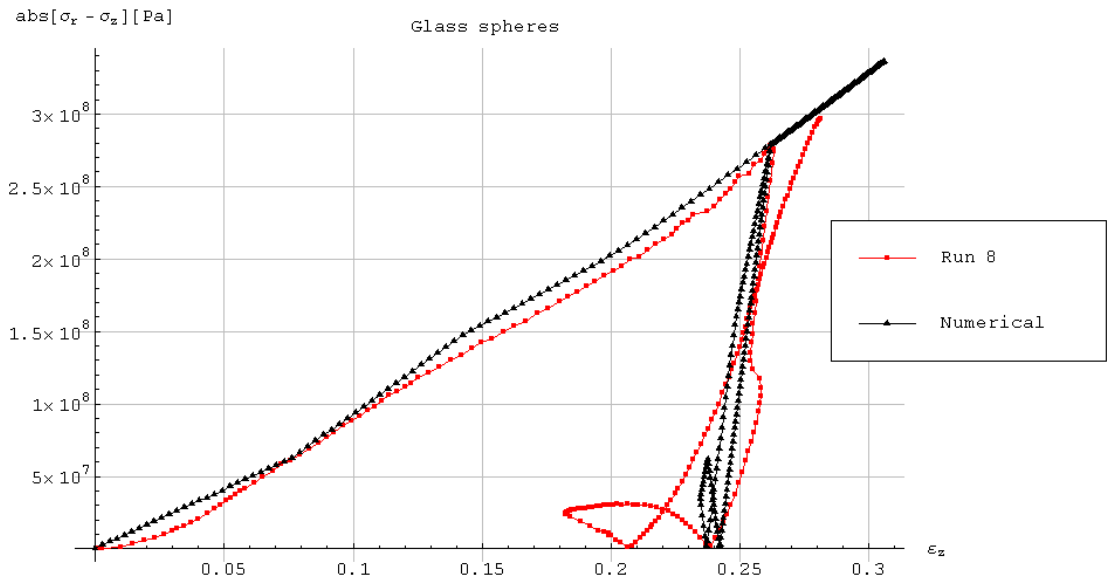

Figure 11.17: Mises stress as a function of axial strain in the sample for experimental and numerical results.

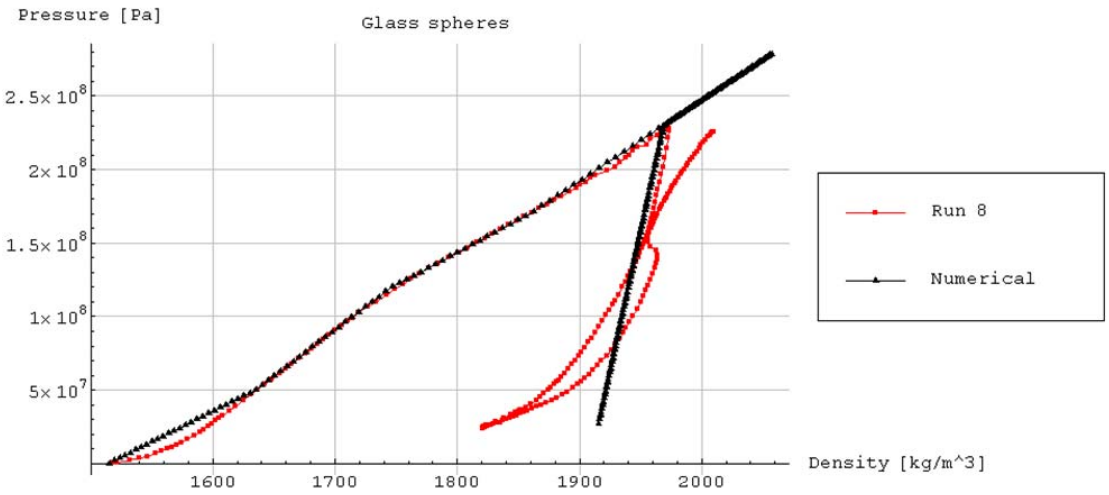

Figure 11.18: Pressure as a function of density for experimental and numerical results.

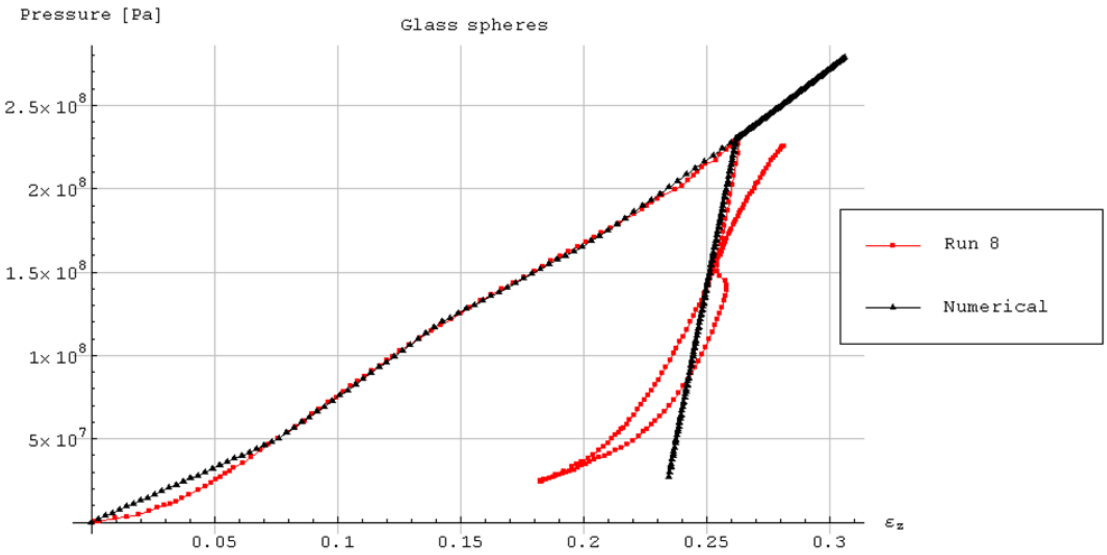

Figure 11.19: Pressure as a function of axial strain in the sample for experimental and numerical results.

Run 9

Specific properties for this run were as following. Mass of sample was 0.005738 kg and initial height of sample was 0.01645 m. The maximum displacement used in the numerical analysis before unloading was -0.0037 m, and the displacement at reloading was -0.00331 m.

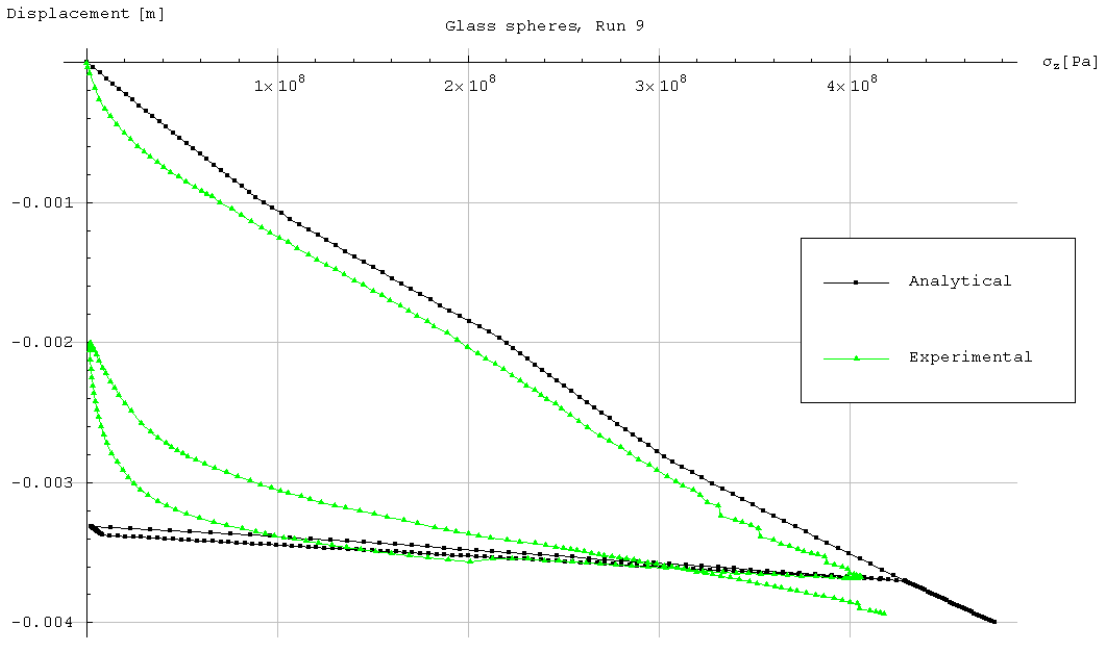

Figure 11.20: Displacement used in numerical analysis vs. experimental measurements.

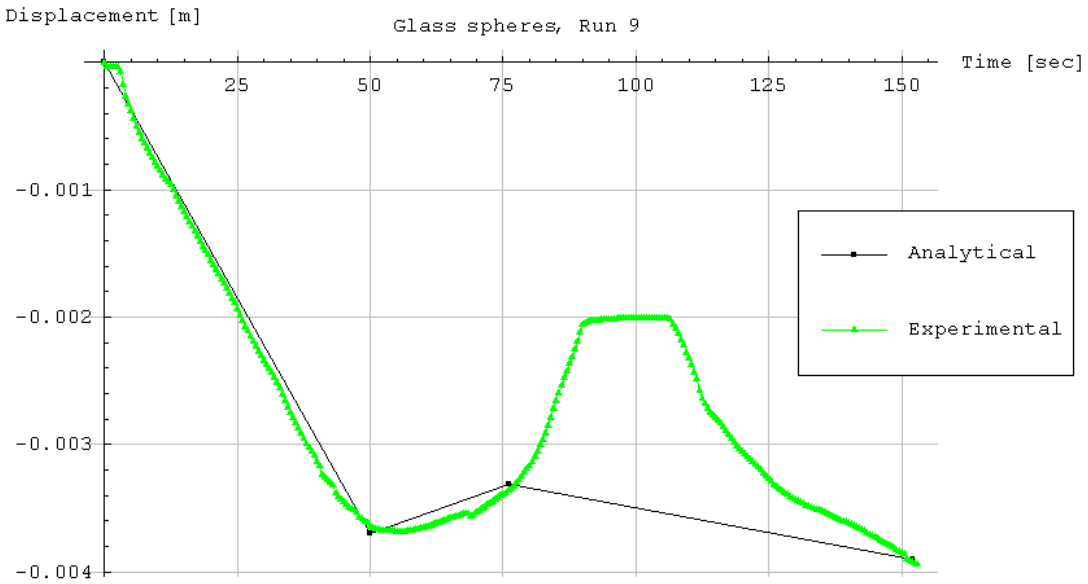

Figure 11.21: Displacement as a function of time.

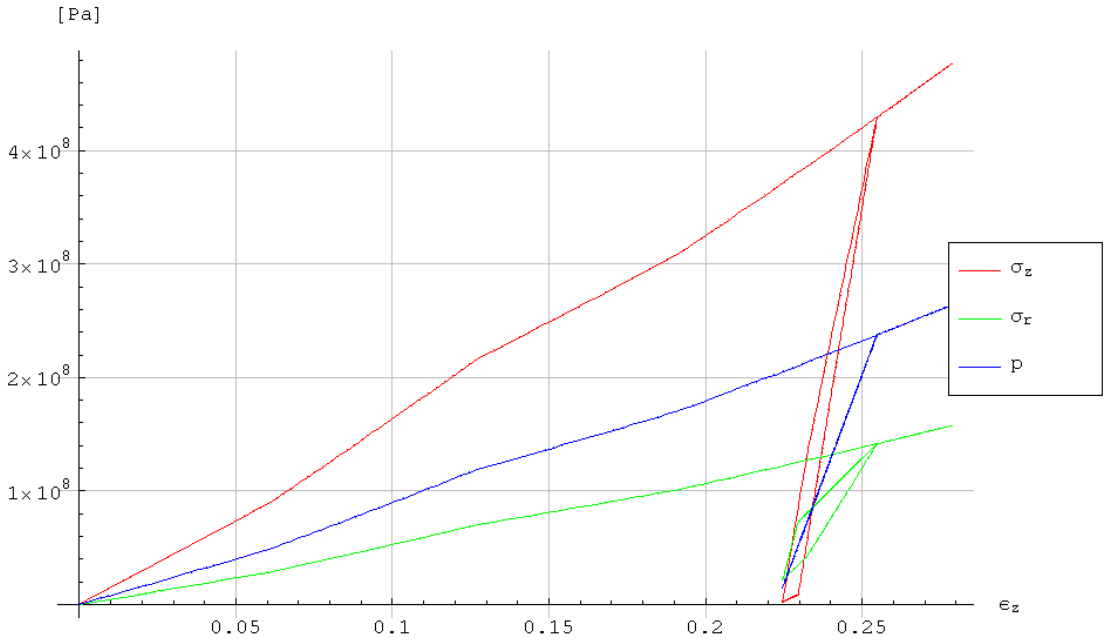

Figure 11.22: Numerical results of pressure, axial stress and the radial stress as a function of the axial strain in the sample.

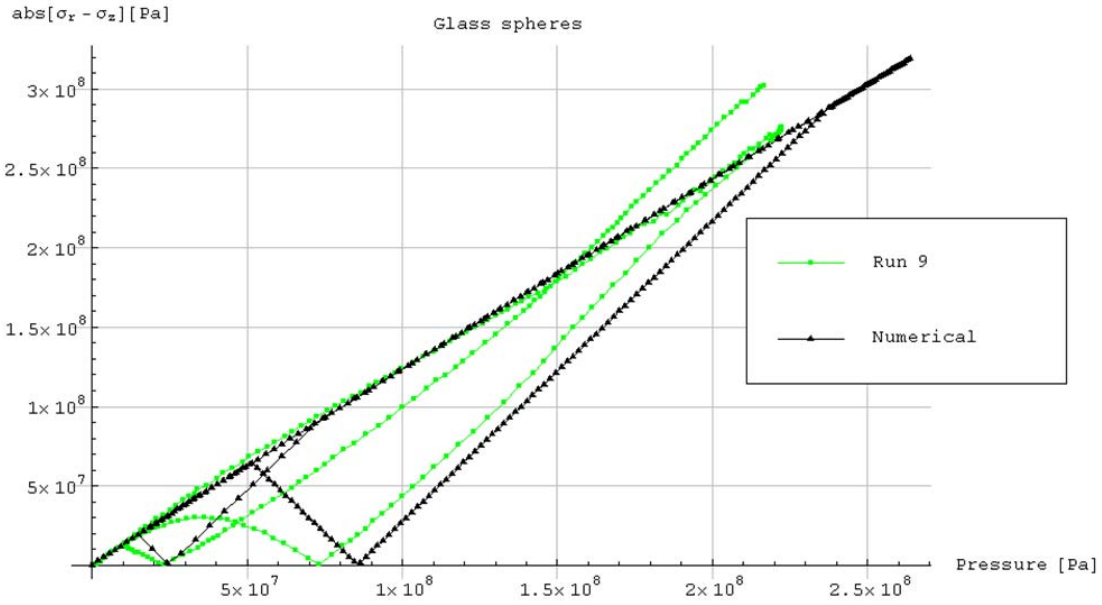

Figure 11.23: Mises stress as a function of pressure for experimental and numerical results.

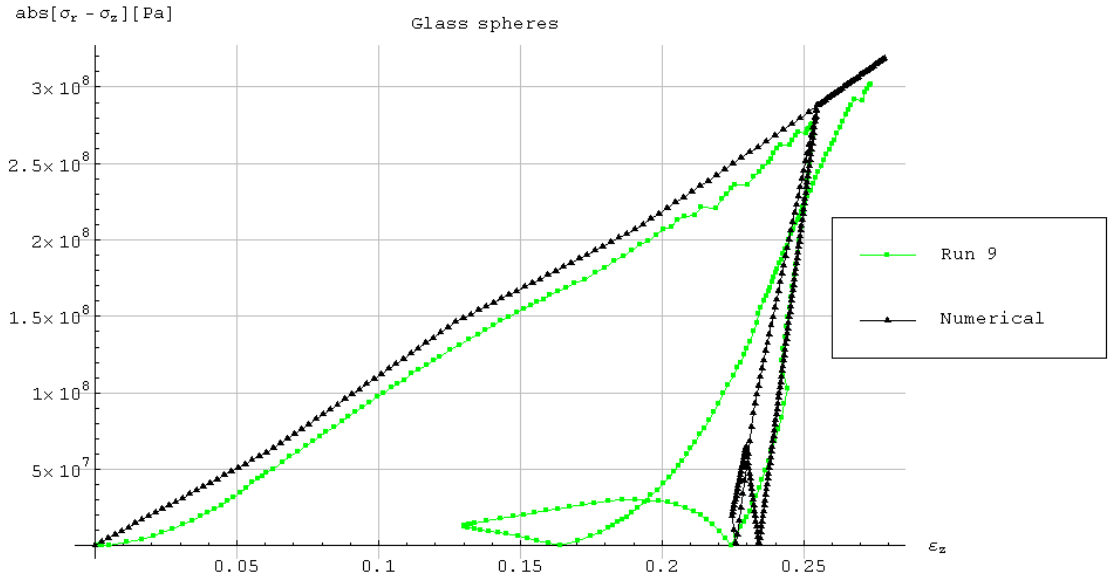

Figure 11.24: Mises stress as a function of axial strain in the sample for experimental and numerical results.

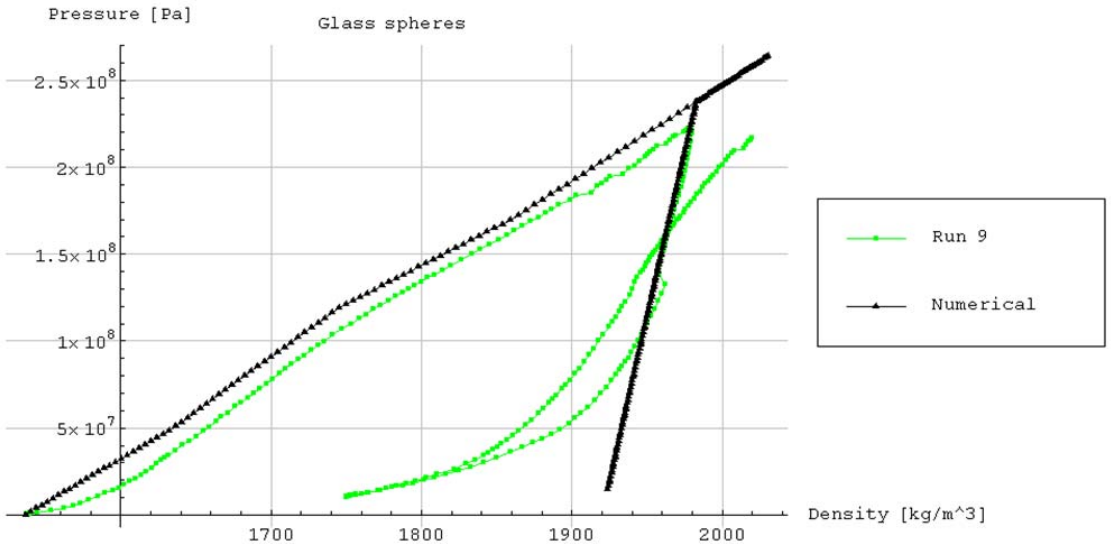

Figure 11.25: Pressure as a function of density for experimental and numerical results.

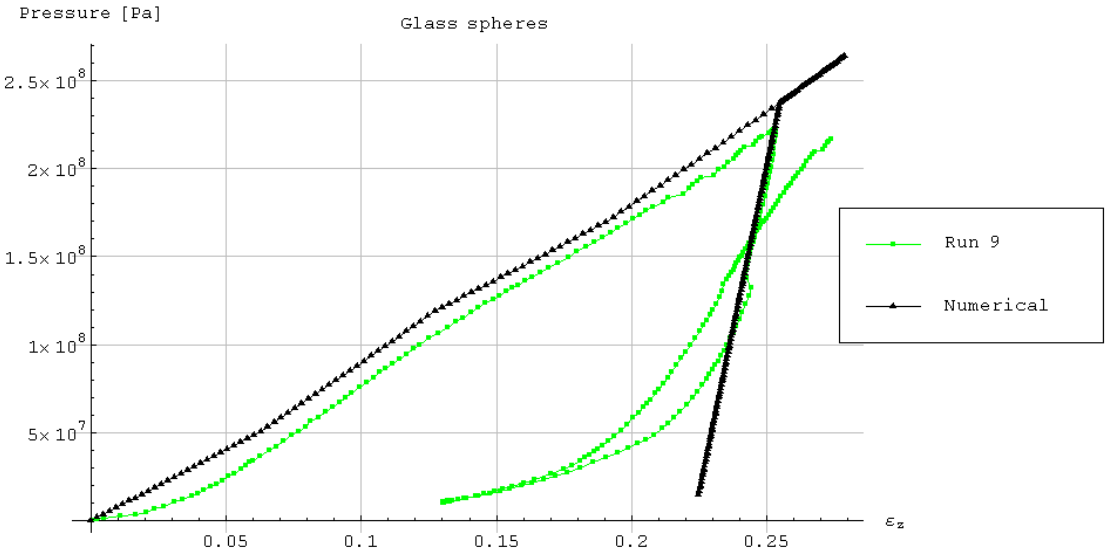

Figure 11.26: Pressure as a function of axial strain in the sample for experimental and numerical results.

Run 10

Specific properties for this run were as following. Mass of sample was 0.005738 kg and initial height of sample was 0.01645 m. The maximum displacement used in the numerical analysis before unloading was -0.00275 m, and the displacement at reloading was -0.00234 m.

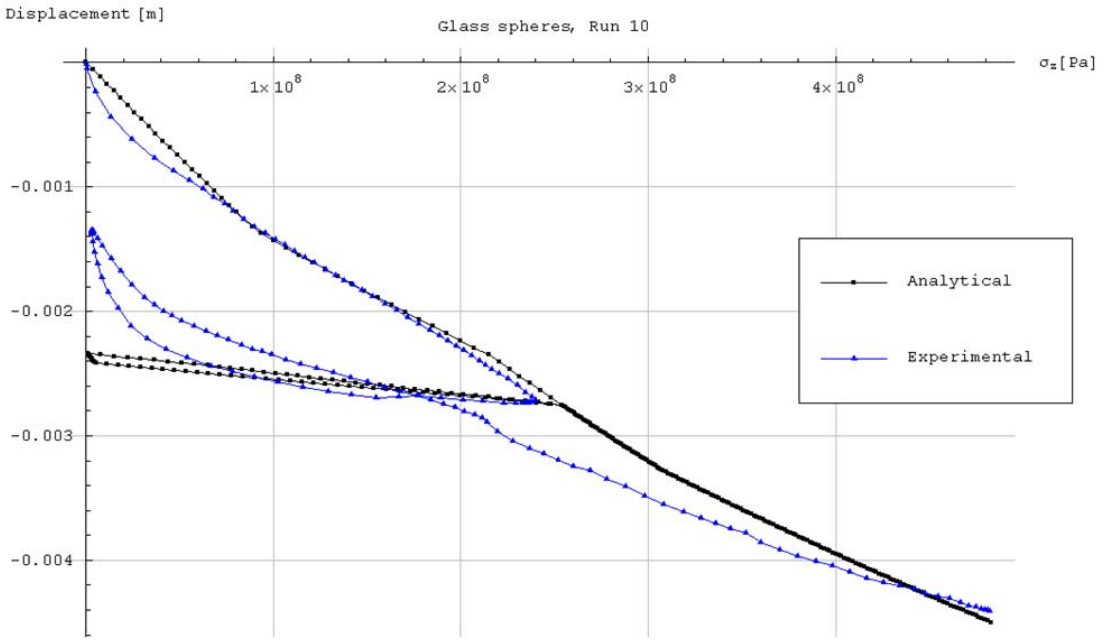

Figure 11.27: Displacement used in numerical analysis vs. experimental measurements.

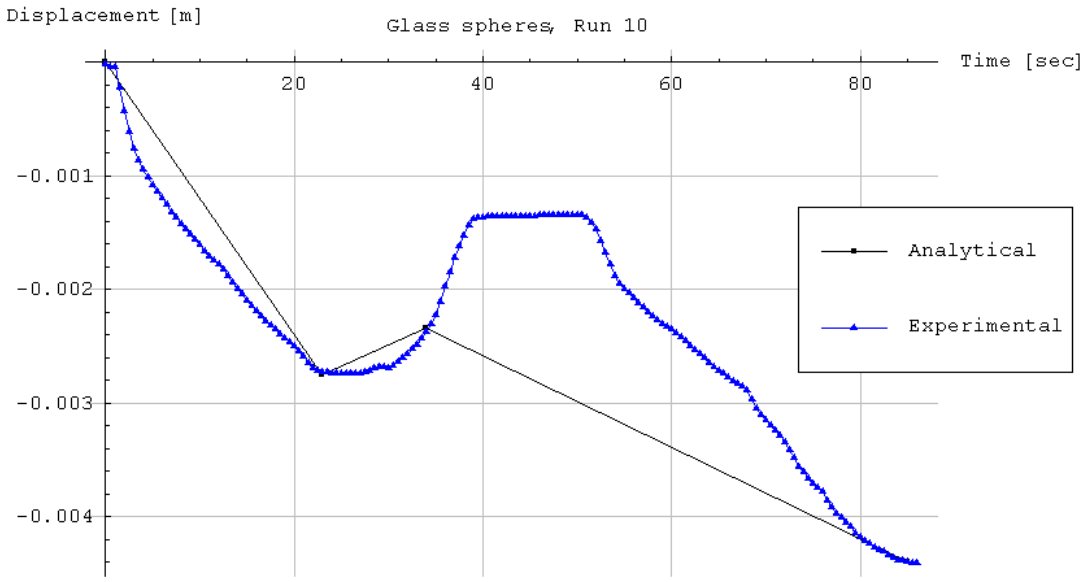

Figure 11.28: Displacement as a function of time.

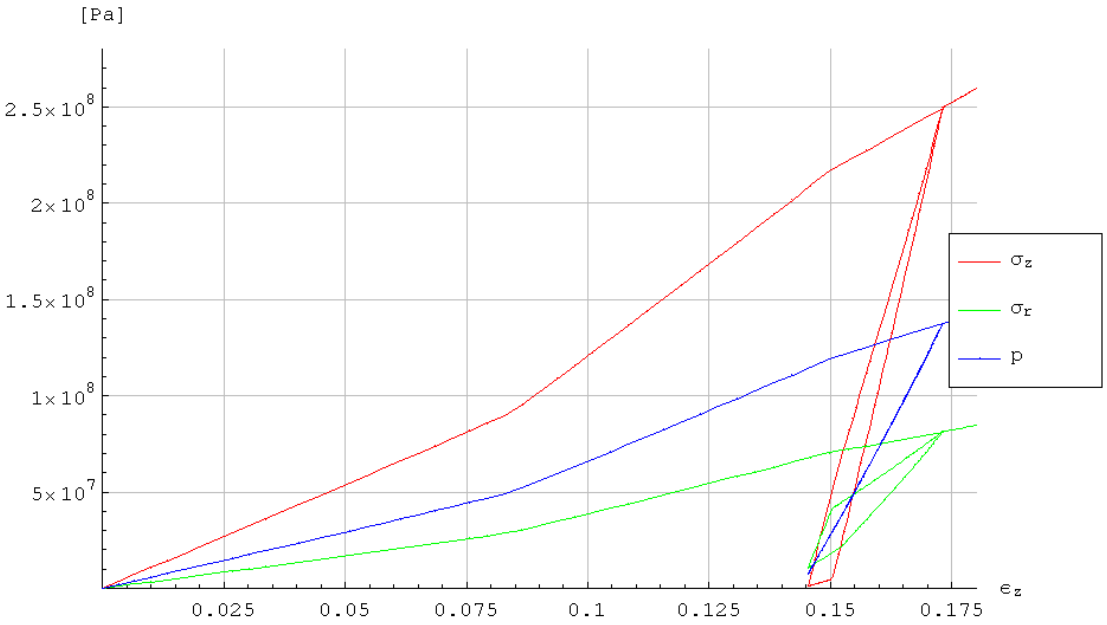

Figure 11.29: Numerical results of pressure, axial stress and the radial stress as a function of the axial strain in the sample.

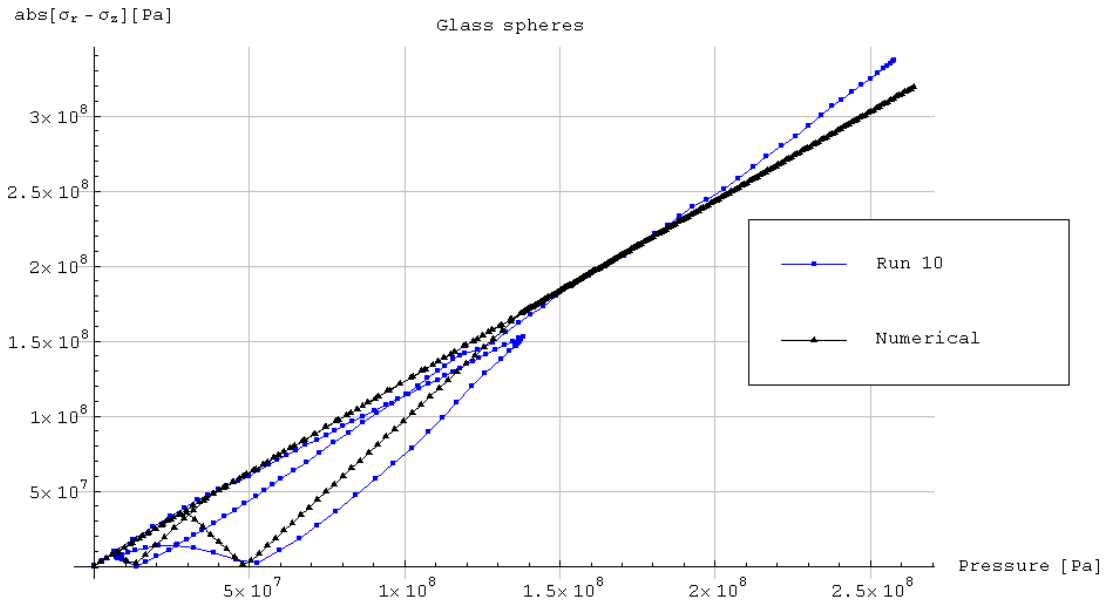

Figure 11.30: Mises stress as a function of pressure for experimental and numerical results.

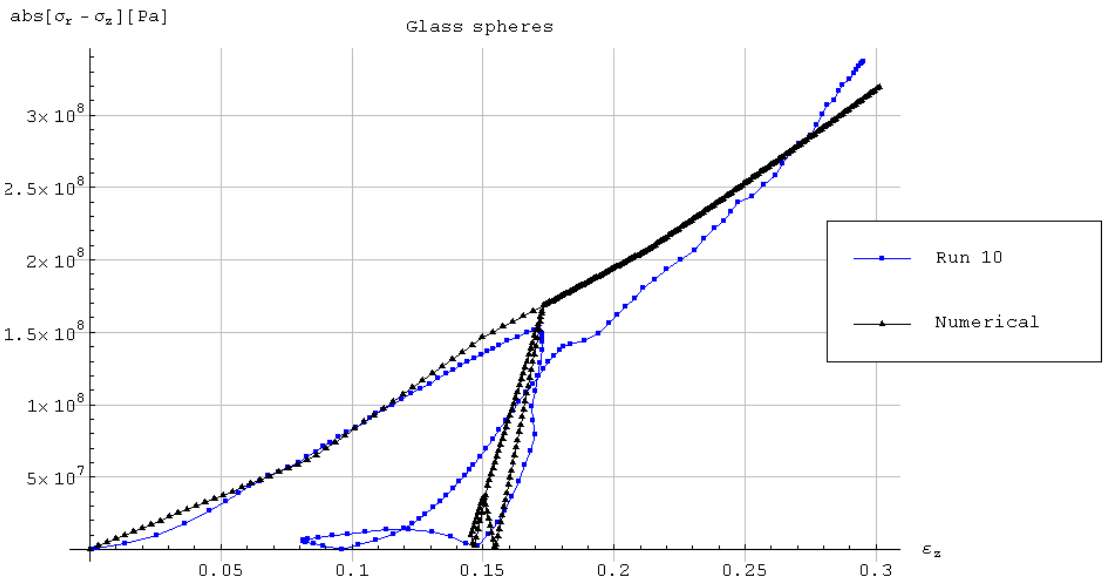

Figure 11.31: Mises stress as a function of axial strain in the sample for experimental and numerical results.

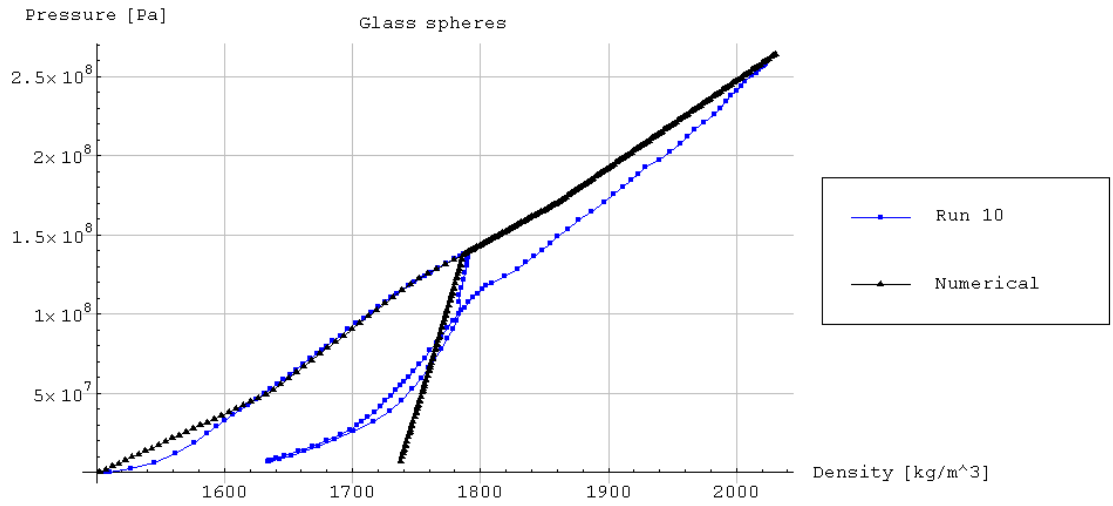

Figure 11.32: Pressure as a function of density for experimental and numerical results.

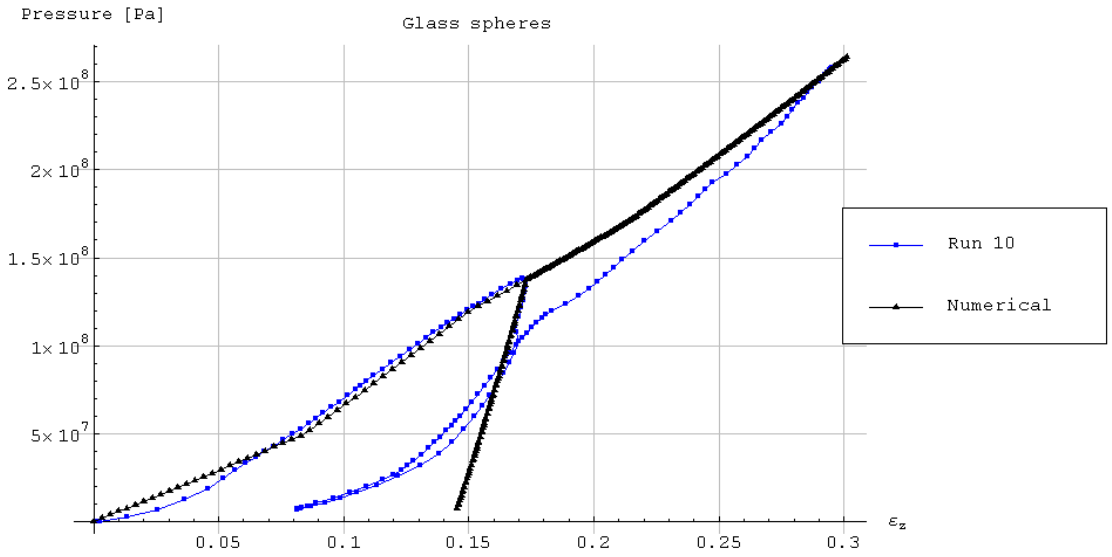

Figure 11.33: Pressure as a function of axial strain in the sample for experimental and numerical results.

12 Simulations

To test whether the experimental values for the aluminum sample in section 5.2 was trustworthy a finite element analysis (FEA) was conducted. The software used for the FEA is called COSMOSWorks and is a design analysis tool attached to SolidWorks (CAD software).
A linear elastic isotropic model was used for the materials. For the steel cylinder an elastic modulus of 210 GPa and a Poisson's ratio of 0.29 were used. The elastic modulus, *E*, and Poisson's ratio was set to 71.7 GPa and 0.33 for the aluminum (Alloy 7075-T6).

Figure 12.1 shows the setup for the FEA and is similar to the experimental test setup. An axial stress of 400 MPa was applied to the upper surface of the aluminum sample. The lower surface of the aluminum sample is fixed in the y-direction (axial direction) while it is allowed to move in z- and x-direction without friction. The upper and lower pistons were thus not modeled. The steel cylinder's lower surface is fixed in all directions (see figure 12.1). The mesh used for this study had a global element size of 3.5 mm (figure 12.2). A finer local mesh of 1 mm was used on the inner cylindrical surface of the steel cylinder and the cylindrical surface of the aluminum sample.

The hoop and axial strain (figure 12.4 and 12.5) was calculated by the FEA at the outer surface of the steel cylinder at the axial center position of the aluminum sample to be $\varepsilon_\theta = 3.825\ 10^{-5}$ and $\varepsilon_z = 2.799\ 10^{-5}$. Inserting this into equation (4.20) gives $\sigma_r(r = r_1) = -83.76$ MPa while the FEA gives $\sigma_r(r = r_1) = -117.8$ MPa. Thus we conclude that equation (4.20) does not hold for the very low radial expansion of the aluminum test sample. Using equation (5.3) we get the Poisson's ratio

$$\nu' = \frac{k}{1+k} = \frac{\sigma_r}{\sigma_z + \sigma_r} = \frac{-83.76}{-400 - 83.76} = 0.173$$ or using the FEA value for σ_r that gives 0.235.

Thus equation (5.3) does not hold either since the true value is 0.33. In figure 12.7 and 12.8 the axial and hoop strain for experimental and FEA is compared. The hoop strain shows a small discrepancy between measurements and FEA result.

In addition we also modeled the FEA with the pistons. We studied both long and short pistons. The results were the same (not shown), but the agreements with experiments were not so good as without pistons. Even when the lower surface of the aluminum sample was fixed in the y-direction (axial) and friction between the aluminum surface and the pistons was zero, we did not find as good agreement as the FEA without pistons. Notice that the contact condition between the lower aluminum and piston surface was set to "No penetration". Also the pistons were set to have no interactions with the surrounding steel cylinder. Figures 12.9-12.11 shows the setup and results for this FEA. The hoop and axial strain for this FEA case was $\varepsilon_\theta = 3.635\ 10^{-5}$ and $\varepsilon_z = 2.096\ 10^{-5}$ at the outer surface of the steel cylinder at the center of the aluminum sample. These strains are compared with the measurements and the other FEA in figure 12.7 and 12.8.

We do not know why the two FEA analyses give different results. Physically they should give the same results, but obviously the contact algorithm between the lower aluminum surface and the piston surface in some way influence the simulation results.

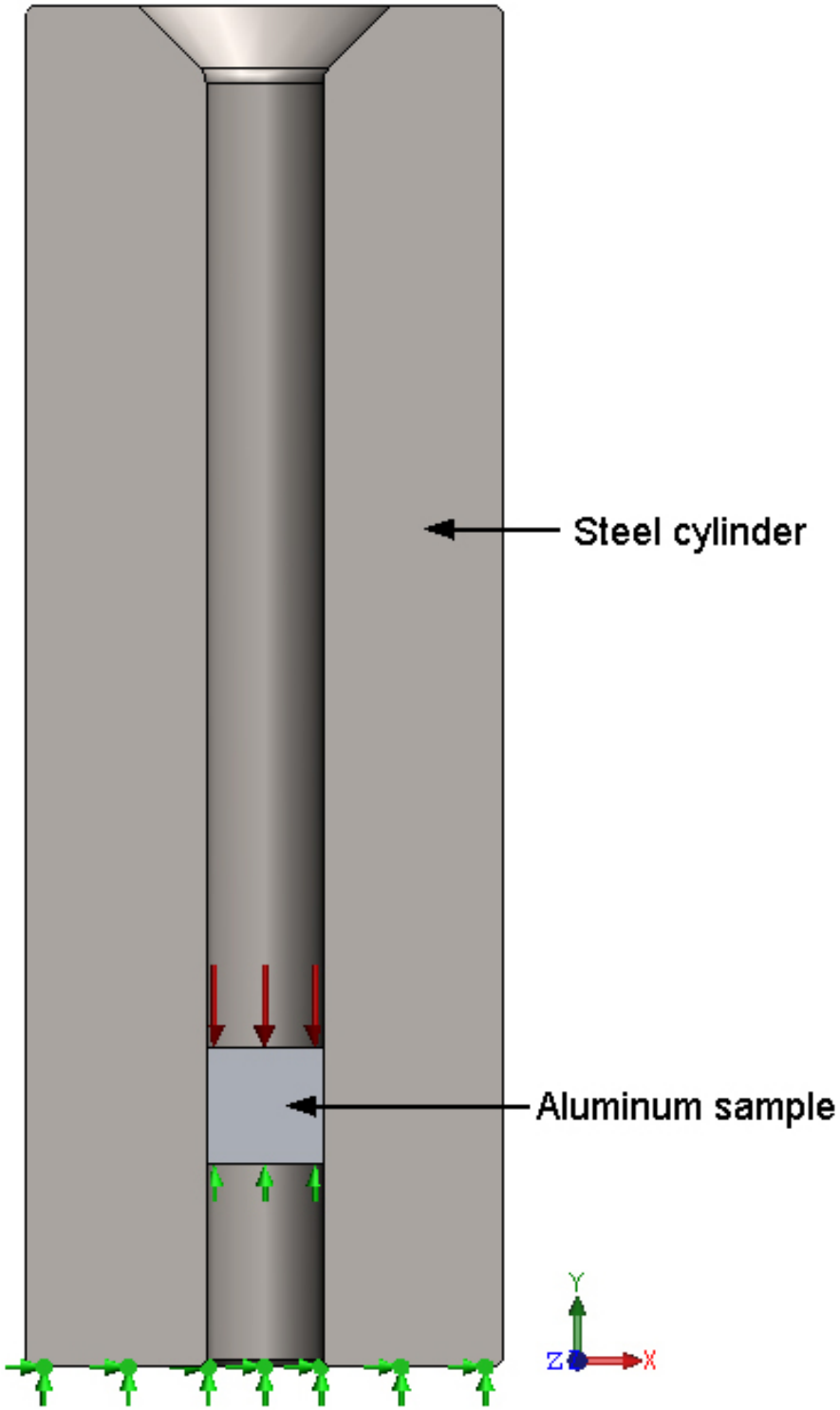

Figure 12.1: Restraints and load condition for the simulation.

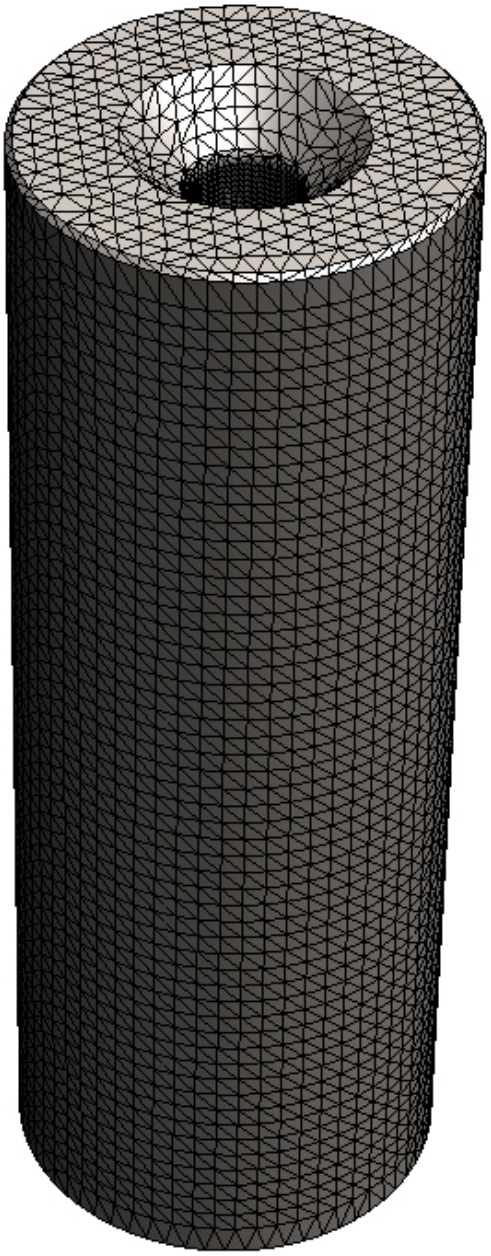

Figure 12.2: Mesh for the FEA.

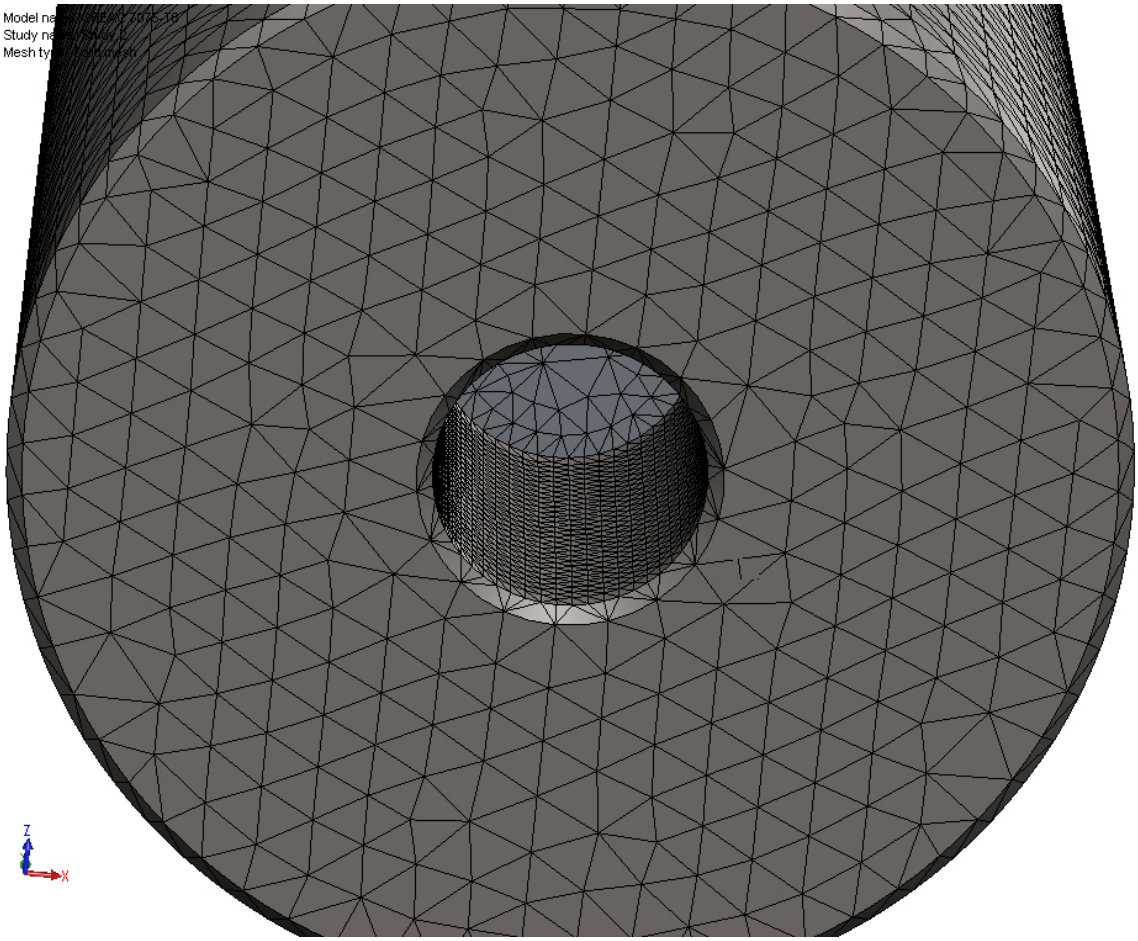

Figure 12.3: Close up view of the fine mesh inside the steel cylinder and the aluminum sample.

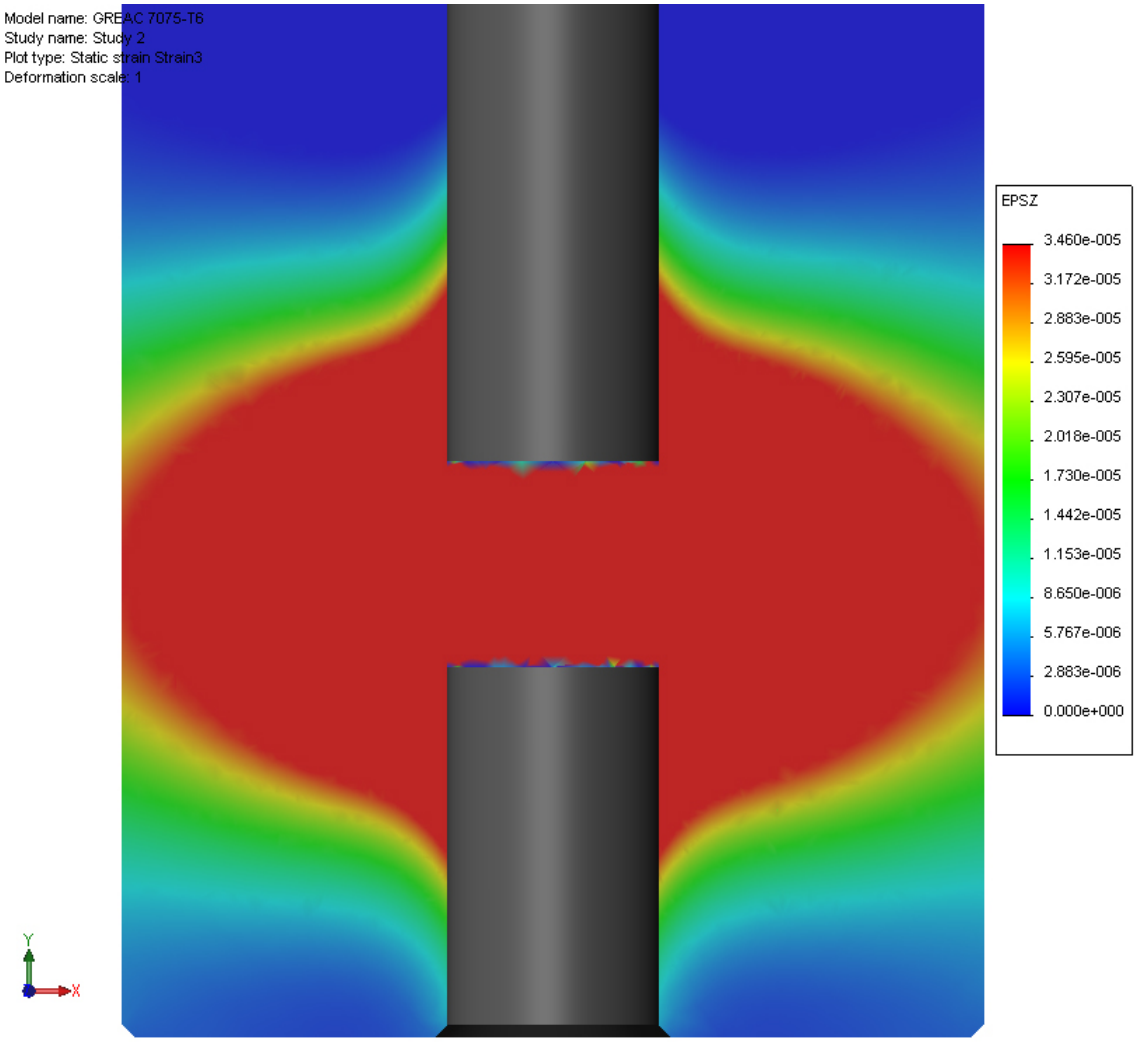

Figure 12.4: Strain in the z-direction (hoop).

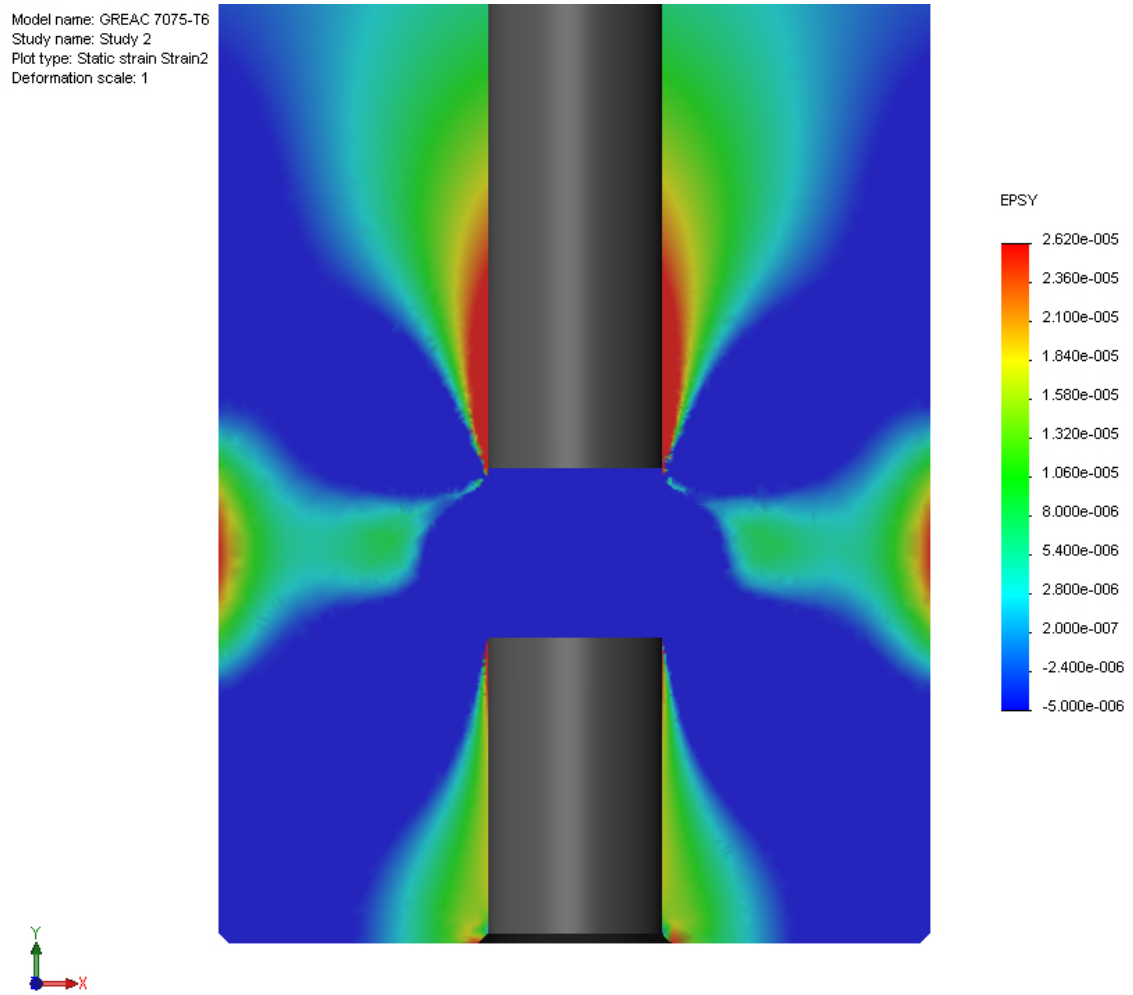

Figure 12.5: Strain in the y-direction (axial).

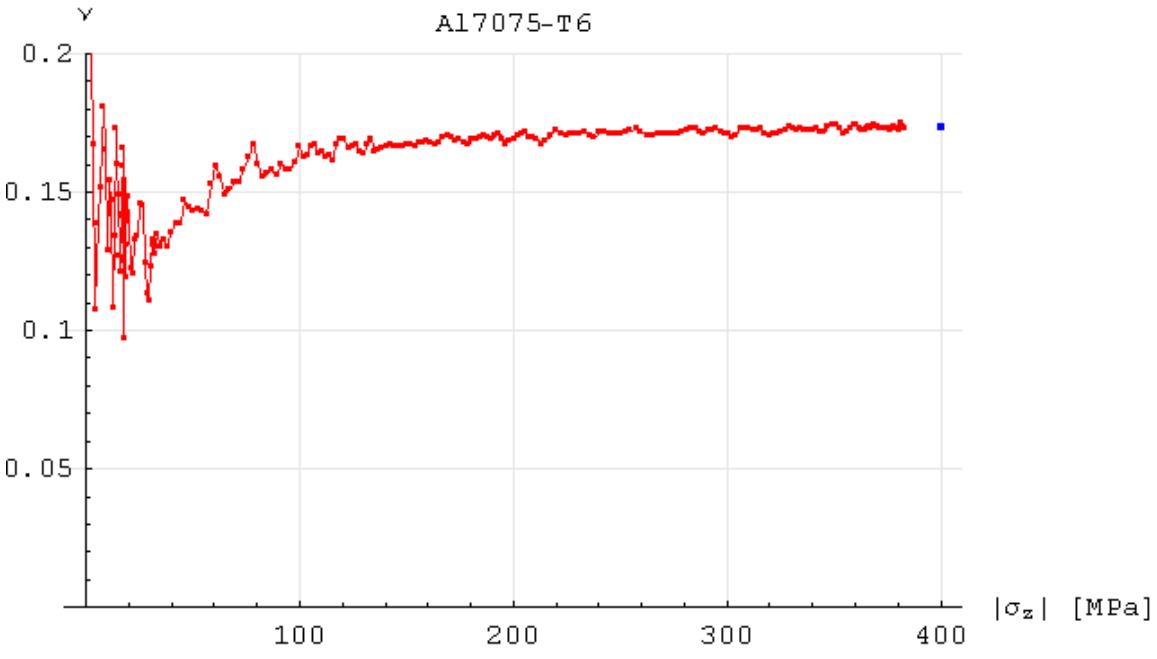

Figure 12.6: Poisson's ratio vs. axial stress. ■ Experimental, ■ FEA.

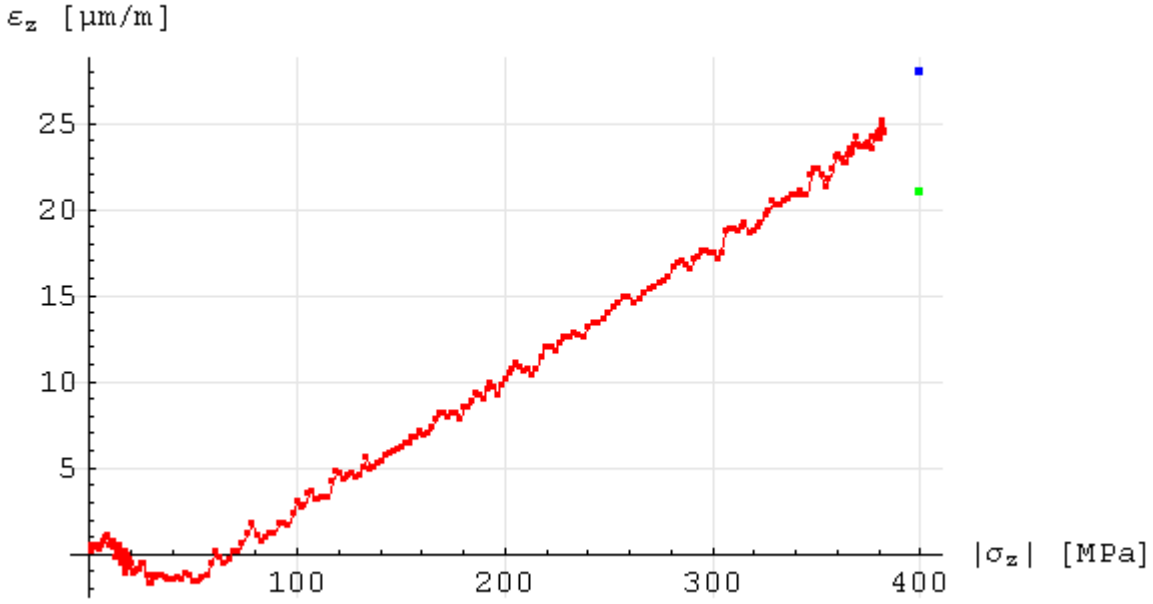

Figure 12.7: Axial strain vs. axial stress. ■ Experimental, ■ FEA without pistons, ■ FEA.with pistons.

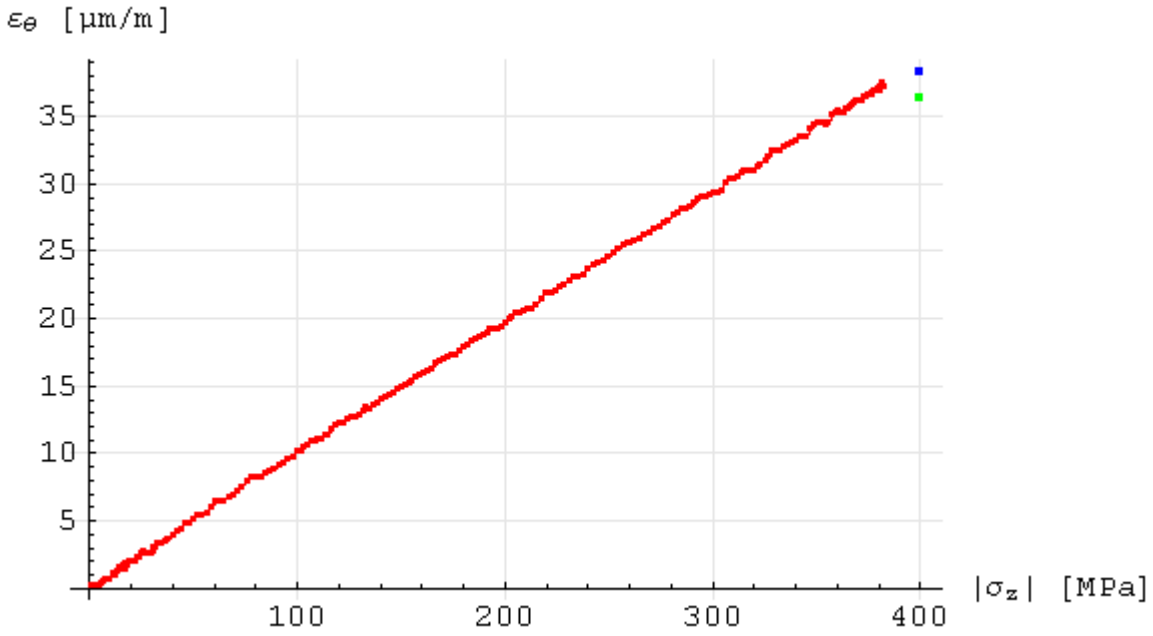

Figure 12.8: Hoop strain vs. axial stress. ■ Experimental, ■ FEA without pistons, ■ FEA with pistons.

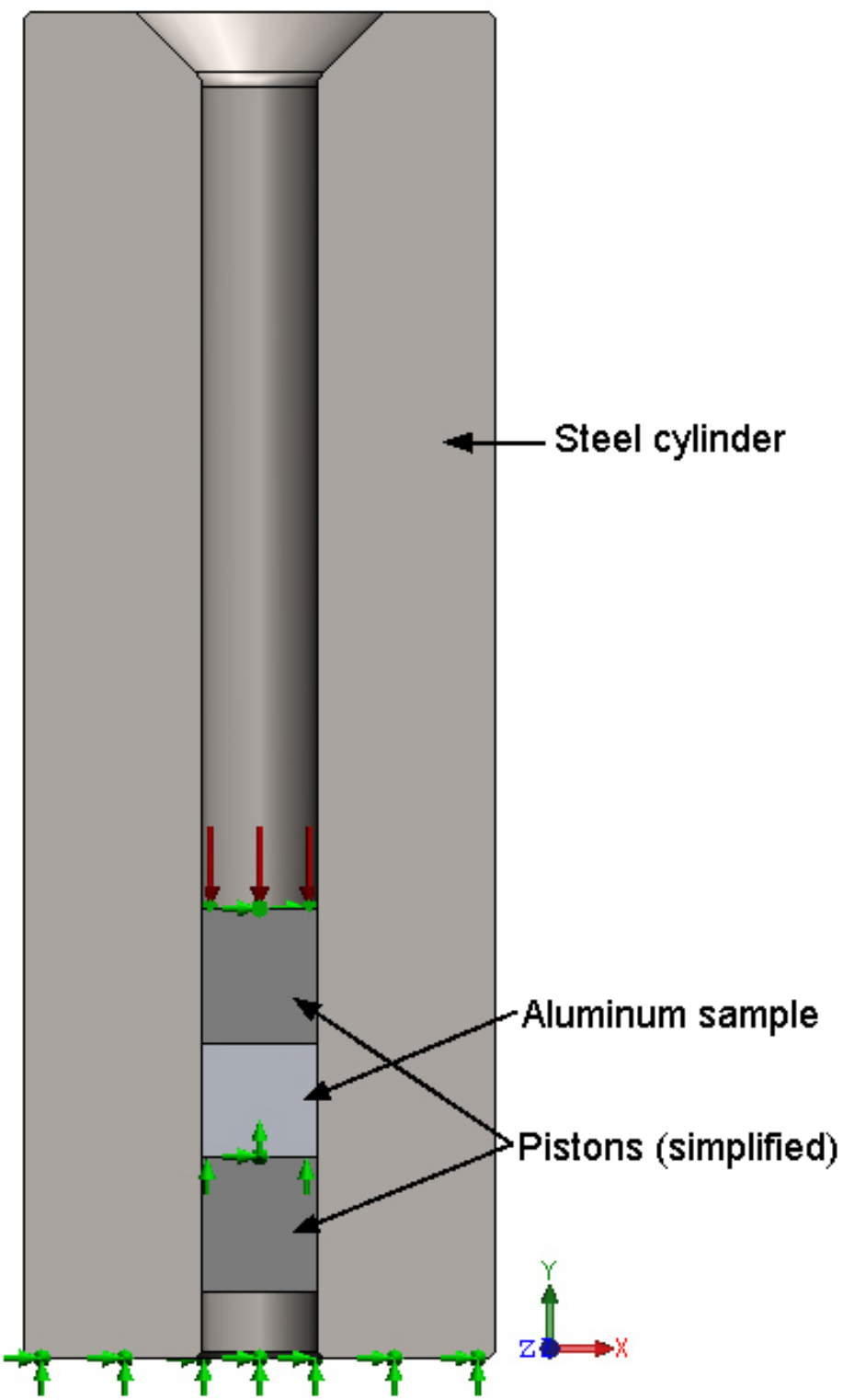

Figure 12.9: Restraints and load condition for the FEA simulated with short pistons. The lower aluminum surface is locked in the y-direction (axial).

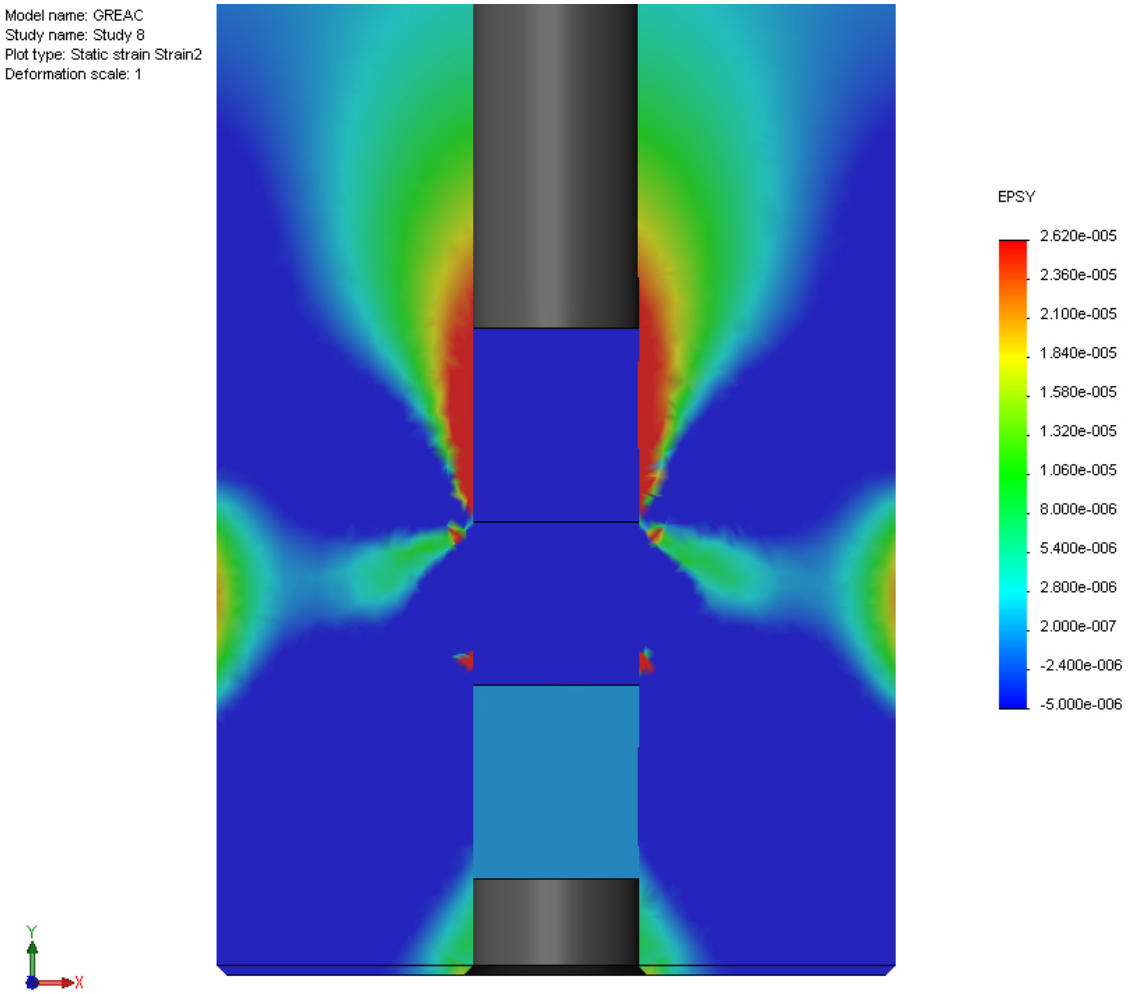

Figure 12.10: Strain in the y-direction (axial) when modeling with two pistons

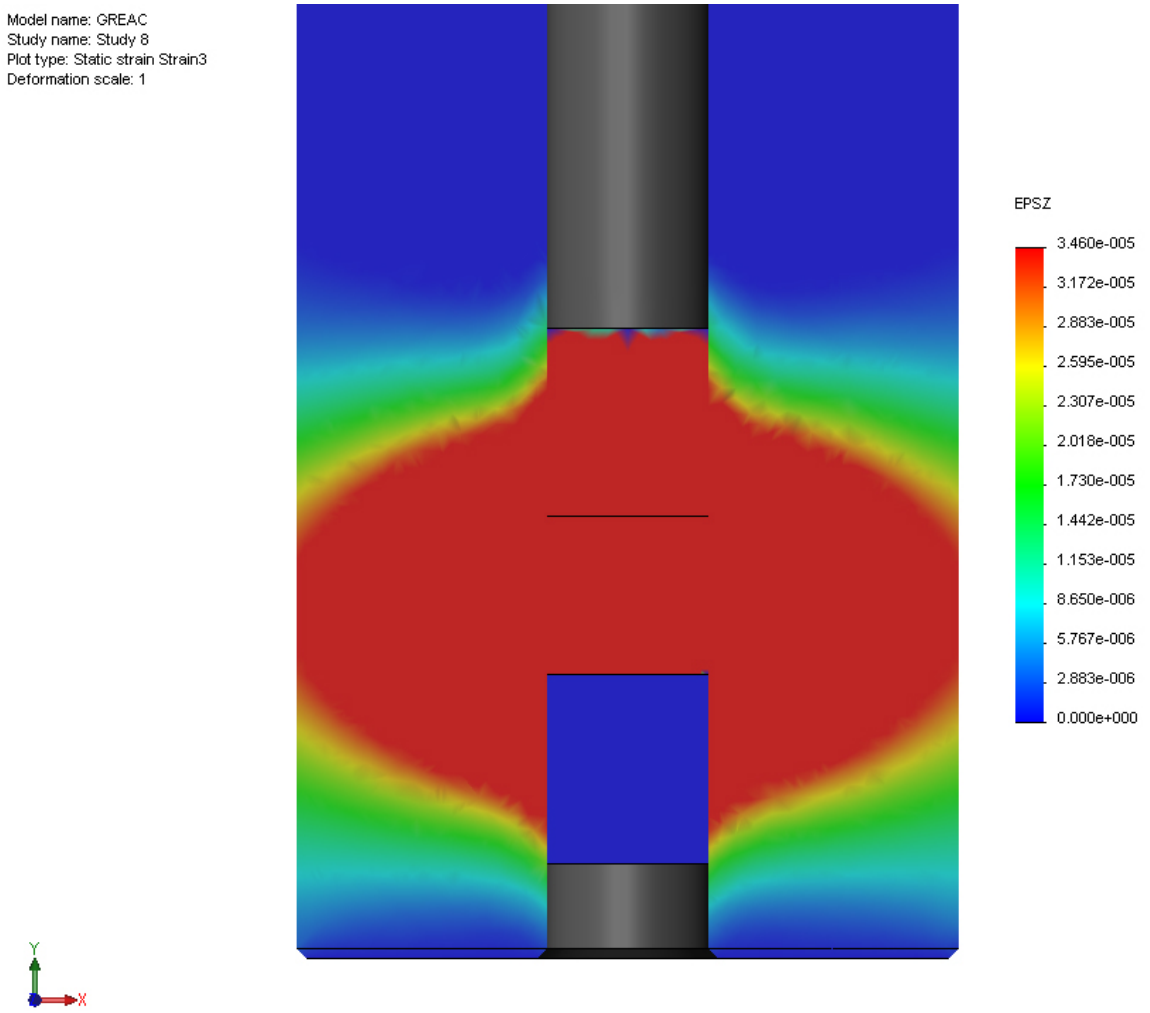

Figure 12.11: Strain in the z-direction (hoop).

13 Conclusion/discussion

In this report a theoretical and experimental study of a glass powder (diameter of 40-80 μm) is made to establish a constitutive material model by using the GREAC (Gauged REActive Confinement) cell. We show how an algorithm can be used to establish constitutive material models from the output data from the experiment. The algorithm use measurements of the axial force, the axial displacement of the glass powder and the axial and hoop strain measured at the outer surface of the GREAC cell. A finite element analysis has been performed by using SolidWorks with the COSMOSWorks design analysis tool. We did find some discrepancies in two finite element analyses for setups that should give the same results. We believe that the main reason for this is the functionality of some contact algorithm in COSMOSWorks.

References

(1) Teland J. A., Svinsås E.: "Everything you wanted to know about material testing but were afraid to ask", FFI/Rapport-2003/00155

(2) Stanojevic M., "A comparison of two test methods for determining elastomer physical properties", Polymer Testing 3 (1983), pp. 183-195

Appendix A Material properties and geometry of the steel cylinder

Young's modulus: E= 2.06 10^{11} Pa,
Poisson's ratio, $\nu = 0.29$,
Geometry: R_1=8.5 mm, R_2=35 mm.

Appendix B Material properties of natural rubber

Shear modulus: G= 1.2 10^5 Pa, [Ref. 2].
Poisson's ratio, $\nu = 0.4998 \pm 0.1$, [Ref. 2].

Appendix C Material properties of the piston

Young's modulus: E= 2.06 10^{11} Pa,
Poisson's ratio, $\nu = 0.29$,
Geometry, upper piston: l_0=0.31 m.